Single-molecule detection of transient dimerization of opioid receptors 1: Homodimers' effect on signaling and internalization

Peng Zhou[1], Taka A. Tsunoyama[1], Rinshi S. Kasai[2,3,4], Koichiro M. Hirosawa[4], Ziya Kalay[5], Amine Aladag[1], Takahiro K. Fujiwara[5], Simone Pigolotti[6], and Akihiro Kusumi[1,5]

[1]Membrane Cooperativity Unit, Okinawa Institute of Science and Technology Graduate University, Onna-son, Okinawa 904-0495, Japan. [2]Institute for Life and Medical Sciences, Kyoto University, Kyoto 606-8507, Japan. [3]Division of Advanced Bioimaging, National Cancer Center Research Institute, Tokyo 104-0045, Japan. [4]Institute for Glyco-core Research (iGCORE), Gifu University, Gifu 501-1193, Japan. [5]Institute for Integrated Cell-Material Sciences (WPI-iCeMS), Kyoto University, Kyoto 606-8501, Japan. [6]Biological Complexity Unit, Okinawa Institute of Science and Technology Graduate University, Onna-son, Okinawa 904-0495, Japan.

Abstract

Opioid receptors (ORs) are critical for endogenous and synthetic analgesics. Their homodimerization is considered important for their pharmacological diversities, but whether they form homodimers remains controversial. Here, we established that the three classical ORs, μ-, κ-, and δ-ORs (MOR, KOR, and DOR, respectively) undergo repeated transient (120-180 ms) homodimerizations every few seconds. This was done by using single-molecule imaging and developing theories for analyzing single-molecule colocalization data, which provide the key parameters, homodimer-monomer dissociation equilibrium constants and rate constants. Their 9-26 amino-acid C-terminal cytoplasmic domains, without sequence similarities, are involved in specific homodimerization, whereas the transmembrane domains provide less specific affinities. Using the membrane-permeable peptides mimicking the C-terminal homodimerization sequences which block homodimerizations, functions of monomers and homodimers were dissected. KOR and DOR homodimers, but not MOR homodimers, activate downstream G-proteins differently from monomers upon agonist addition, without influencing OR internalization. These findings could guide strategies to enhance OR-based analgesia.

Introduction

Three classical opioid receptors (ORs), μ-, κ-, and δ-ORs (MOR, KOR, and DOR, respectively), are distributed across the central and peripheral nervous systems and play important roles in regulating pain perception, hedonic homeostasis, mood, and well-being.[1, 2] ORs are prototypical class A G-protein-coupled receptors (GPCRs), and serve as key receptors for a variety of endogenous and synthetic analgesics. These OR subtypes play critical roles in pain therapeutics, and at the same time, in the development of tolerance to and dependence on analgesics, which are likely associated with activations of the inhibitory G-protein and β-arrestin pathways in complex manners.[2, 3, 4]

The diversity of OR conformations and their interactions with other proteins not only drives various cellular physiological responses but also contributes to a spectrum of brain circuit responses, both beneficial and adverse.[4, 5, 6, 7] Hence, a profound understanding of the mechanisms by which ORs' distinct downstream responses are induced is essential for the development of analgesic drugs with minimized side effects. In addition, receptor dimerization and clustering are often key steps for triggering the downstream signaling cascades in other receptor signaling.[8]

The pharmacological diversities of ORs might be enhanced by their propensity to form homodimers[9, 10] and heterodimers.[11, 12, 13] Agonist-induced homodimer formation significantly influences the balance of MOR's downstream G-protein and β-arrestin pathways.[14] Other studies suggested that dimerization, both homo and hetero, might modulate or be modulated by biased agonism, highlighting its significance in receptor signaling (for example, see Refs[15,16] for homodimers and Refs[17, 18] for heterodimers). For the β2-adrenergic receptor, another class A GPCR, homodimers are responsible for generating the basal receptor signal in the absence of agonists, a key common characteristic of GPCRs.[19] Furthermore, OR heterodimerization is important for their cooperative functions, as supported by functional and pharmacological studies.[17, 20] Therefore, understanding both the homo- and hetero-dimerizations of ORs, as well as those of other class-A GPCRs, is fundamental to deciphering their functional regulation mechanisms.[16, 21, 22, 23, 24, 25]

Despite such extensive research, the very existence of homo- and hetero-dimers of ORs, particularly at physiological expression levels, remains controversial.[26] Previous detection of homodimers of DOR,[9, 27, 28] MOR,[27, 28] and KOR,[13, 28] and heterodimers of all OR pairs[28] contrasts with recent single-molecule imaging studies. These studies, performed at physiological expression levels in the plasma membrane (PM) of living cells, in contrast to the results obtained under the conditions of overexpression in cells and very high concentrations in vitro, which are often necessary for the use of bulk observation methods, showed that MOR,[29, 30] DOR,[30] and KOR[31] are predominantly monomeric. Therefore, they concluded that previously observed dimerization and its functional and pharmacological consequences would be artifacts due to the employment of very high OR concentrations. Meanwhile, other single-molecule investigations detected the nanodomains of KOR and MOR[32] as well as the transient MOR dimerization[33] or that only after the agonist DAMGO binding, but not morphine.[14]

To address the overexpression issue and resolve these controversies, determining the dimer-monomer equilibrium constant K_D is imperative, as it is unaffected by the expression levels. In addition, since several GPCR homodimers are apparently metastable with lifetimes on the order of 0.1-1 s,[19, 21, 33, 34, 35, 36, 37] estimating the dimer dissociation and association rate constants, k_{off} and k_{on}, respectively, is essential for establishing the comprehensive description of the dynamic dimer-monomer equilibrium of ORs. Such insights would enable us to unequivocally determine whether ORs form homo- and hetero-dimers and to what extent under various expression conditions, including both the lower and higher regions of physiological expression levels in different cells in various brain regions. Furthermore, identifying specific binding sites for homo- and hetero-dimerizations, given the high amino acid similarities among the three classical ORs, would be interesting from the protein-interaction viewpoint and highly beneficial for developing reagents that modify dimerizations.

In the present research, we addressed these issues, using advanced single-molecule imaging, tracking, and analysis. The single-molecule approach was selected for its ability to directly visualize receptor molecules' dimerization and dissociation in living cells. To extract the dimer-monomer equilibrium constant, K_D, and rate constants, k_{off} and k_{on}, from single-molecule imaging data, we developed two novel theories: one to evaluate k_{off} from the

96 distribution of single-molecule colocalization durations (instead of intuitive methods employed
97 previously), and another to estimates K_D (k_{on} can be calculated as k_{off}/K_D).
98 We present our findings in two back-to-back papers. This paper focuses on
99 homodimers, while the companion paper addresses heterodimers.[38] In this paper, we report
100 that all three ORs engage in continual, repeated, transient homodimerizations at 37°C, with
101 K_Ds of 5.87 ± 0.56, 15.24 ± 1.54, and 16.42 ± 0.53 copies/μm^2 for KOR, MOR, and DOR,
102 respectively. The homodimer lifetimes are in the range of 120-180 ms (dimer dissociation rate
103 constants in the range of 6.71 to 8.47 s^{-1}), unequivocally demonstrating that even at low
104 physiological expression levels, the three ORs form transient homodimers. Furthermore, we
105 identified that the ≈9-26 amino acid sequences in the cytoplasmic C-terminal domains,
106 without sequence similarities, are involved in the distinct homodimerizations of the three ORs,
107 in line with the previous DOR homodimerization data,[9] whereas the transmembrane domains
108 might promote both homo- and heterodimerizations in a less specific manner, in partial
109 agreement with previous results.[21, 39, 40, 41, 42]
110 Building on these amino-acid sequences, we developed peptides that suppress OR
111 homodimerization within live cells. This has allowed us to distinguish the functions of OR
112 dimers from monomers, which could not be done before. OR monomerization by these
113 peptides enhances and diminishes agonist-induced signals downstream from G proteins for
114 KOR and DOR, respectively, without influencing agonist-induced internalization. Meanwhile,
115 monomerization had no discernible effect on MOR signaling or internalization. These findings
116 may inform novel strategies in developing more effective and safer pain treatments.

Results

All three ORs continually interconvert between transient homodimers and monomers: analysis by colocalization index based on the pair cross-correlation function (PCCF)

ORs conjugated with the SNAPf tag protein at their N-termini (SNAPf-ORs) were expressed in the PM of CHO-K1 cells, which do not express ORs.[43] These SNAPf-tagged molecules were functional (Supplementary Fig. 1a, b) and labeled with the fluorescent membrane-impermeable SNAP ligands, SNAP-Surface 549 and SNAP-CF660R, with 60% and 61% efficiencies, respectively (Supplementary Fig. 1c-e). For the experiments examining OR homodimerization, we simultaneously labeled a SNAPf-OR (for example, SNAPf-KOR) with both SNAP-Surface 549 and SNAP-CF660R so that the number densities of the two probes on the PM were about the same, with spot densities of 0.5 ± 0.25 spots/μm^2 for each color (total spot number densities of 1.0 ± 0.5 spots/μm^2; for conciseness, we will describe as ≈1 spot/μm^2 throughout this report), and then performed simultaneous dual-color single-molecule observations at normal video rate (30 Hz) at 37°C, using a home-built total internal reflection fluorescence (TIRF) microscope.[44, 45]

Virtually all of the SNAPf-OR fluorescent spots exhibited diffusion in the PM, but in addition, they often exhibited temporary colocalization and co-diffusion,[37] suggesting the frequent formation of transient homodimers (Supplementary videos 1 and 2; Fig. 1a). We focused on simultaneous two-color experiments, due to the ease of image analysis. For the single-color imaging data, see Supplementary Fig. 2a, b, which show an example of repeated homodimerizations of a KOR molecule with different partner KOR molecules, consistent with the observations made with other GPCRs.[35, 36, 37]

To quantitatively examine the extent of the colocalization of two single molecules, we employed a "colocalization index", which parameterizes the propensity of a pair of magenta and green molecules to become localized within 100 nm. Namely, the colocalization index is defined from the pair cross-correlation function (PCCF) histogram for the SNAP-Surface 549 (green) and SNAP-CF660R (magenta) spots (Fig. 1b),[46] as the ratio of PCCF (0-100 nm) vs. PCCF (400-500 nm) (Supplementary Fig. 2c-e). When a molecular interaction does not exist, the colocalization index is equal to one within experimental uncertainty. When it does exist,

147 the index becomes significantly greater than 1. As a negative control (including incidental
148 colocalization), the 180°-rotated magenta image was superimposed on the green image (see
149 Supplementary Fig. 2d, grey histogram in Fig. 1b), providing a colocalization index of ≈1.
150 KOR, MOR, and DOR exhibited significantly higher colocalization indexes than the negative
151 controls (Fig. 1c), suggesting that they form homodimers (and possibly greater oligomers
152 when the expression levels are enhanced).
153

154 **Homodimer dissociation rate constant k_{off} (inverse of the dimer lifetime) can be**
155 **obtained from single-molecule colocalization experiments**

156 To evaluate the homodimer lifetimes, each time we found the colocalization event of spots
157 with different colors within a threshold distance R = 200 nm (see Supplementary Note 1,
158 which shows that the selection of R does not affect the measured k_{off} value, although it could
159 affect its SEM),[36, 37, 44, 45] its duration was measured. By measuring the durations of >1,500
160 events (in ⩾17 cells; all statistical parameters are summarized in Supplementary Table 1),
161 we obtained the distribution of colocalization durations (Fig. 1d).
162 To evaluate the homodimer dissociation rate constant k_{off} (inverse of the homodimer
163 lifetime) from the distribution of colocalized durations, we developed a theory based on the
164 diffusion equation that predicts the distribution of colocalization durations (Supplementary
165 Note 1). The crucial result of this theory is that, from the histogram of the *colocalization*
166 durations, we can rigorously estimate the homodimer dissociation rate constant k_{off} and thus
167 the homodimer lifetime τ_2. This result holds despite the fact that the generally used
168 colocalization threshold distance is ≈200 nm, which is much greater than the molecular scale
169 of 3~10 nm. The theory shows that, at a time resolution of 33 ms and under the conditions
170 of quite limited signal-to-noise ratios in our experiments, the histogram of the colocalization
171 durations can be fitted with the sum of two exponential functions, where the two decay
172 constants represent the incidental colocalization lifetime ($1/\alpha$) and the inverse of the
173 dissociation rate constant ($1/k_{off}$).
174 Previously, we[36, 37, 45] and others[33, 34, 35] depended on intuitive methods to obtain the
175 homodimer lifetimes from optical colocalization data. However, due to the theory developed

here, we now have a firm basis to obtain the homodimer dissociation rate constant k_{off} from the distribution of single-molecule colocalization durations.

Brief outline of the theory to evaluate k_{off} from the single-molecule colocalization duration distribution (Supplementary Note 1)

In dual-color single-molecule tracking, a colocalization is defined as an event in which two spots are located closer than a threshold distance R. Starting from the 2D diffusion equation, we found that the distribution of the dwell times in the threshold circle without binding (incidental lifetime τ_{inci}; i.e., incidental colocalization duration, Fig. 1e) is expressed by

$$p_d(t) \approx \sum_{n=1}^{\infty} \frac{2D\epsilon{\mu_n}^2}{R^3} e^{-\frac{D{\mu_n}^2 t}{R^2}} \approx \alpha e^{-\alpha t} \quad , \tag{9}$$

where D is the diffusion coefficient, R is the threshold distance, ε is a regularization factor, and μ_n is the n-th real positive 0 of the Bessel function (Equation numbers in the main text are matched with those in Supplementary Note 1 and 2 for easy reference). Under our experimental conditions, the first term is sufficient to describe the distribution, providing a single exponential function with a decay time constant of $R^2/D\mu_1^2 = 1/\alpha$, which is the incidental colocalization lifetime (τ_{inci}). We indeed found that the colocalization time distribution for incidental colocalizations obtained for the overlay on the 180°-rotated image (Supplementary Fig. 2d) could be fitted with a single exponential function (using both Akaike's and Bayesian information criteria; AIC and BIC, respectively) (Fig. 1d).

The dwell time in the threshold circle with binding (T; i.e., colocalization duration, Fig. 1e) is given by the sum of τ_{inci} added to the sum of multiple binding durations, τ_i.

$$T = \tau_{\mathrm{inci}} + \sum_{i=1}^{n} \tau_i \quad . \tag{10}$$

Here, the terms in the sum correspond to possible multiple binding events during a dwell; i.e., to obtain the correct k_{off} value, we will need to consider the cases where the observed colocalization durations are the results of multiple binding events.

Combining these results, we obtain the dwell time distribution in the threshold circle.

$$P(T) = \frac{\alpha k_{\mathrm{off}}}{\Gamma}\left\{\left[1 - \frac{(\Delta - \Gamma)}{2k_{\mathrm{off}}}\right] e^{-\frac{T}{2}(\Delta-\Gamma)} - \left[1 - \frac{(\Delta + \Gamma)}{2k_{\mathrm{off}}}\right] e^{-\frac{T}{2}(\Delta+\Gamma)}\right\} \quad , \tag{21}$$

where $\Delta = (\alpha + k_{\mathrm{off}} + k_{\mathrm{on}})$ and $\Gamma = \sqrt{\Delta^2 - 4\alpha k_{\mathrm{off}}}$.

At a time resolution of 33 ms and under the conditions of the quite limited signal-to-noise ratios in our experiments, we obtain

$$(\Delta - \Gamma)/2 \approx k_{\mathrm{off}} \quad , \tag{30}$$

$$(\Delta + \Gamma)/2 \approx \alpha \quad . \tag{31}$$

This result explains why the histogram of the colocalization durations can be fitted by the sum of two exponential functions. Most importantly, it permits to identify the two decay constants with the incidental colocalization lifetime ($1/\alpha = \tau_{inci}$) and the inverse of the dissociation rate constant ($1/k_{\mathrm{off}}$), as anticipated.

OR homodimer dissociation rate constant k_{off} and true homodimer lifetime

As shown in Fig. 1d, we were able to fit the three histograms for KOR, MOR, and DOR, obtained from the correctly overlaid images, with the sum of two exponential functions, as predicted by equations 30 and 31. The fitting provided two time constants, τ_1 and τ_2 ($\tau_1 \leq \tau_2$). The histogram obtained from the rotated overlay images could be fitted with a single exponential function, which provided the time constant τ_{inci} (= $1/\alpha$) (the numbers of significant exponential terms were always confirmed by both AIC and BIC in this work). We found that $\tau_1 \approx \tau_{\mathrm{inci}}$ for all three ORs. The longer decay time constant obtained from the histogram for the correctly overlaid images (τ_2) provides k_{off} (= $1/\tau_2$; Supplementary Note 1). As such, using this theory, by simply plotting the histogram of the colocalization durations, we can obtain the correct homodimer dissociation rate constant k_{off} (by taking account of the multiple binding-dissociation cycles).

The homodimer lifetimes of KOR, MOR, and DOR were estimated to be 178 ± 5, 122 ± 3, and 120 ± 3 ms, respectively, from the histograms shown in Fig. 1d (after correction for the trackable duration lifetimes of the two fluorescent probes). These lifetimes are considerably shorter than that reported for KOR (≈1.8 s at room temperature, perhaps ≈20°C).[33] This difference might be predominantly explained by the lower temperatures employed in the previous study (20°C), whereas our observations were performed at 37°C. In addition, it is possible that our imaging and analysis methods are more sensitive to short-term colocalization events, compared with previous investigations.

228

229 **Determination of OR homodimer-monomer equilibrium constant (K_D) from PCCF**

230 In the literature, the question of whether ORs (or GPCRs or any other membrane proteins)
231 form homodimers or not has been extensively debated. However, the facts of the matter are
232 that many membrane proteins would form homodimers and clusters anyway at higher
233 expression levels, and that the physiological expression levels vary greatly from cell to cell.
234 Therefore, the critical point should be to quantitatively estimate the homodimer affinity; i.e.,
235 to evaluate the homodimer dissociation (homodimer-monomer) equilibrium constant K_D.
236 Here, we developed a theory (Supplementary Note 2) for evaluating K_D from the PCCF of the
237 OR fluorescently-labeled in two colors (PCCF in the form of a histogram, as shown in Fig. 1b
238 and Supplementary Fig. 2e), under conditions where the expression levels are low and so the
239 presence of oligomers greater than dimers could be neglected. The K_D values evaluated from
240 the PCCF by this method are quite accurate because we employed the expression conditions
241 of ≈1 fluorescent spot/μm^2 (Supplementary Fig. 3c, e): Within this range, the colocalization
242 index barely depended on the expression levels when K_D >6.5 copies/μm^2 (see the simulation
243 results shown in Supplementary Fig. 3a-e, particularly Supplementary Fig. 3c). At these copy
244 number densities, we hardly detected oligomers greater than dimers.

245 The values of K_D were 5.87 ± 0.56, 15.24 ± 1.54, and 16.42 ± 0.53 copies/μm^2 for
246 KOR, MOR, and DOR at 37°C, respectively (Fig. 2a and b; K_D was first determined for each
247 movie using the PCCF and the number of fluorescent spots obtained from the movie, fixed
248 fluorescent labeling efficiencies of 0.60 for SNAP- SNAP-Surface549 and 0.61 for SNAP-
249 CF660R, and fitting parameters of K_D and the precision of overlaying two-color movies plus
250 single-molecule localizations for the two fluorescent probes, and then the arithmetic mean (±
251 SEM) K_D was obtained using K_Ds determined for all the movies; the number of movies are
252 provided in Supplementary Table 1, like other statistical parameters). These K_D values mean
253 that KOR is more likely to exist as homodimers than MOR and DOR (the main results are
254 summarized in Table 1 and their statistical test results are in Supplementary Table 1). Our
255 estimated values of K_D for the MOR and KOR homodimers found here exhibited much smaller
256 errors compared with previous estimates (for MOR,[33] 27.43 ± 11.75 copies/μm^2; and for
257 KOR,[30] 32 ± 15 copies/μm^2), and their mean values are smaller by factors of approximately

258 1.7 and 4.9, respectively. In contrast, these K_D values are greater than the K_D's of β2AR and
259 FPR homodimers (1.6 and 3.6 copies/μm^2, respectively).[19, 37] The K_D values for CD28, the
260 constitutive disulfide-linked dimer control molecule,[47] and the transmembrane domain of the
261 LDL receptor (TM^{LDLR}), the monomer control molecule,[37] are 0.041 ± 0.072 and 132 ±21
262 copies/μm^2, respectively, providing the basic dynamic range (4400x) for this method to
263 evaluate K_D values (although the value for CD28 is a nominal value, representing the
264 experimental limitation). Our results indicate that the KOR homodimer affinities are higher
265 than those of DOR and MOR, and thus partially explain previous data showing that KOR, but
266 not DOR or MOR, forms homodimers at low membrane densities.[30] In the following part of
267 this report and in the companion paper, we use the colocalization index when showing the
268 direct experimental data is preferrable, whereas we show the K_D values when providing the
269 fundamental constants is desirable. Under our standard experimental conditions, the
270 colocalization index is simply related to K_D as shown in Fig. 2c, and K_D can be roughly
271 evaluated using the graphs shown there, although we performed actual fitting for the PCCF
272 for each cell to obtain the K_D value for each cell (the final K_D value and its SEM were obtained
273 as the arithmetic mean of the K_Ds for all the observed cells).

274 Using k_{off} and K_D, k_{on} can be calculated as k_{off}/K_D (equation 1). Direct determination of
275 k_{on} from single-molecule movies is only possible when the labeling efficiency is 100%. This is
276 because the fluorescent spots that appear to be monomers (protomers) of A and B molecules
277 might be dimers of labeled and non-labeled molecules. For the correction to evaluate the
278 actual numbers of protomers, one would need to know K_D, and thus k_{on} cannot be
279 determined independently from K_D. The percentages (in copy numbers) of molecules
280 (protomers) that exist as dimers at various expression levels (number density of molecules)
281 were calculated from the obtained K_D values (Fig. 2d). Their overall variations are in the
282 range of 3.4-59% of protomers in homodimers over the ORs' predicted physiological
283 expression ranges of 0.3 - 10 copies/μm^2.[26, 29, 33]

284 Therefore, substantial amounts of homodimers would exist in various nerve tissues at
285 any time. The expected average protomer copy numbers existing as monomers and
286 homodimers per cell at various expression levels are shown in Fig. 2b and 2d. However, all of
287 these homodimers are forming and dispersing all the time, with lifetimes shorter than 0.2 s

288 (Fig. 1d). Once dissociated into monomers, they will again form homodimers, often with
289 different partner molecules (Supplementary Fig. 2a, b), which will occur more readily at
290 higher expression levels. Therefore, although at any moment, 10-21% of ORs might exist as
291 homodimers at the expression levels we employed (≈1 copy/μm^2), the actual molecules
292 existing as dimers are turning over all the time, and within a few seconds (even at an
293 expression level of 1 copy/μm^2; calculated as $1/k_{off} + 1/[k_{on} \times 1]$), virtually all of the
294 molecules experience the periods of homodimers and monomers.

295 A previous biochemical study detected DOR homodimers[9] and a single-molecule
296 imaging study using a fluorescently-conjugated MOR antagonist detected MOR homodimers,[33]
297 in agreement with our results. Meanwhile, at apparent variance with our results, previous
298 single-molecule examinations demonstrated that MOR and KOR tend to exist as monomers
299 even at 20°C, at expression levels between 0.1 and 0.3 copies/μm^2.[14, 31] Since we employed
300 somewhat higher number densities of ≈1 OR spot/μm^2, the discrepancy might simply be due
301 to the number densities of homodimers found in an image. This underscores the critical
302 importance of evaluating the homodimer-monomer dissociation equilibrium constant K_D,
303 rather than simply detecting homodimers.[37]
304

305 **The 9-26 amino-acid sequences in the C-terminal cytoplasmic domains play**
306 **critical roles in OR homodimerization**

307 To advance our understanding of OR homodimerization mechanism, we determined the OR
308 domains and amino acid sequences responsible for homodimerization. First, we examined the
309 involvement of the extracellular N-terminal domains in homodimerization, using the N-
310 terminal deletion mutants (KOR(Δ1-53), MOR(Δ1-51), and DOR(Δ1-35)). Given that the
311 amino-acid homologies in the N-terminal domains among the three ORs are quite low
312 (Supplementary Fig. 4a), we considered a possibility that they might be used to distinguish
313 particular homo- and/or hetero-dimers. These amino-acid sequence ranges were selected
314 partly because the removal of the entire N-terminal extracellular domains blocked the OR
315 expression in the PM, probably due to the deletion of the signal sequences. In addition, these
316 deletion mutants were previously used in X-ray crystallography studies to determine the
317 structures of the remaining parts of ORs.[48, 49, 50, 51]

318 The N-terminal deletion mutants of the three ORs all exhibited diffusion behaviors
319 similar to those of the wild types (without immobilization or clustering) and virtually the same
320 colocalization indexes as those of the wild types (Fig. 1c). These results clearly indicate that
321 the N-terminal extracellular domains are not responsible for homodimerization (see the
322 companion paper about the N-terminal domain involvement in heterodimer formation).
323 We next examined the involvement of the C-terminal cytoplasmic domains. Their
324 amino-acid homologies are also low, and in addition, a previous biochemical analysis
325 indicated that the 15-amino acid stretch in the C-terminal domain is responsible for DOR
326 homodimerization.[9] We examined systematically varied C-terminal deletion mutants (Fig. 3a,
327 b). They hardly exhibited immobility or clustering, and their colocalization indexes showed
328 that KOR's aa 365-380, MOR's aa 358-382, and DOR's aa 357-372 are critical for
329 homodimerization (Fig. 3b and Supplementary Table 1). For DOR, this amino-acid sequence
330 agrees with the previous biochemical data.[9] Meanwhile, the mean colocalization index values
331 never decreased to the index values comparable to those for rotated overlays (≈1) (Fig. 3b)
332 or a monomer control molecule TM^{LDLR} (≈1.1) (Fig. 2a), suggesting the possibility that there
333 might be other weaker homodimerization site(s), which might be the TM domains, as
334 previously suggested for ORs[26, 49, 50, 52, 53] and other class A GPCRs.[21, 39, 40, 41] However, as
335 shown in Supplementary Fig. 4a; the aa identities of TM domains among the three ORs are
336 quite high, and thus the homo-interaction between TM domains might be less specific. We
337 will revisit the TM interactions for homodimerization later.
338 The distribution (histogram) of the colocalization *durations* for each representative
339 deletion mutant, KOR(Δ365-380), MOR(Δ358-382), or DOR(Δ357-372), could be fitted by a
340 single exponential function, rather than the sum of two exponential functions (based on both
341 AIC and BIC). The decay time constants were only slightly longer than the incidental
342 colocalization lifetimes (Fig. 3c); i.e., the τ_2 component, representing the homodimer lifetime
343 fraction, is small and /or the τ_2 is short, and thus the τ_2 component could not be resolved
344 from the incidental colocalization lifetime decay component.
345 By introducing point mutations in these critical regions for homodimerization and their
346 surrounding regions (Fig. 3a), we found that a few to several basic/acidic residues, as well as
347 proline residues, are involved in the OR homodimerization (for particular amino acids, see the

348 colocalization indexes shown in Fig. 3d), suggesting that the electrostatic interactions and the
349 overall structure of the cytoplasmic C-terminal domain could be important for
350 homodimerization. Indeed, the IUPred2 scores (energy-estimation-based predictions for
351 ordered and disordered residues; http://iupred2a.elte.hu)[54, 55] indicated that the C-terminal
352 region could be weakly intrinsically disordered (Supplementary Fig. 4b), and the scores
353 decreased (more ordered) with these point mutations (Supplementary Fig. 4c). Accordingly,
354 in addition to the specific, relatively strong amino-acid interactions, multiple specific, but
355 weak interactions, made possible by the flexible intrinsically disordered regions (IDRs) of the
356 ORs' C-terminal regions, might facilitate the OR homodimerization. Such a mechanism
357 resembling liquid-liquid phase separation was previously found for the dimerization of the
358 transcription factor PU.1.[56] Furthermore, the IDRs in the C-terminal regions might be
359 necessary to bring the specific binding sites closer so that the actual binding can occur.[57]
360

361 **Peptides mimicking the homodimerization sites block homodimer formation**

362 We then examined whether peptides with the same amino-acid sequences as those of the
363 deleted parts of the mutants could block homodimerization. The use of these peptides was
364 critical for unequivocally demonstrating that the specific amino-acid sequences in the C-
365 terminal regions of KOR, MOR, and DOR are responsible for homodimerizations, because the
366 deletion and point mutations might have induced conformational changes of the true
367 homodimer interaction sites, thus inhibiting homodimerization. Furthermore, if we could
368 develop such homodimerization blockers, they could become extremely useful tools to dissect
369 the functions of OR monomers and homodimers, and might inform future developments of
370 more effective analgesic treatments with fewer side effects and less tolerance development.
371 We employed two approaches. The first one involved the expression of peptides with
372 the same amino-acid sequences as those of the deleted parts of the mutants, conjugated to
373 the C-terminus of mGFP (named mGFP-Kpep, Mpep, and Dpep, collectively called mGFP-
374 Xpeps; numbers in parentheses following mGFP-Xpeps indicate the amino-acid residue ranges
375 in the wild-type ORs) in CHO-K1 cells stably expressing SNAPf-KOR, MOR, or DOR,
376 respectively (Fig. 4a, b). The concentration of the cytoplasmic mGFP-Xpep was measured by
377 confocal fluorescence microscopy, based on calibration with various concentrations of purified

378 mGFP protein dissolved in Ham's F12 observation medium in the glass-base dish
379 (Supplementary Fig. 5a; see Methods).
380 The OR homo-colocalization index in the cells expressing various concentrations of
381 mGFP-Xpep in the cytoplasm (homogeneously distributed throughout the cytoplasm; Fig. 4b)
382 exhibited a clear tendency to decrease with an increase of the specific mGFP-Xpep
383 concentration in the cytoplasm from 0 to 7.8 μM for all three ORs (Fig. 4c), whereas the
384 control mGFP-peptides (mGFP-Dpep for KOR and MOR and mGFP-Kpep for DOR) had no
385 effect (Fig. 4c). Consistently, the distributions of the colocalization *durations* in cells
386 expressing 3.8-7.8 μM mGFP-Xpeps could be fitted by a single exponential function, rather
387 than the sum of two exponential functions (based on both AIC and BIC; Fig. 4d), and the
388 decay time constants became similar to those for the C-terminal deletion mutants (compare
389 Fig. 4d with Fig. 3c; Table 1).
390 As the second approach, the K-, M-, and D-peps were conjugated with the fluorescent
391 dye 5-FAM at their N-termini for visualization, and with the TAT sequence (YGRKKRRQRRR)
392 (using a G10 linker sequence) at their C-termini for membrane permeabilization (FAM-Xpep-
393 TAT; see Methods), and added to cells preincubated with 150 μM pyrenebutyrate for 5 min
394 (Fig. 4e, f).[58] The FAM-peptide-TATs exhibited diffuse spatial distributions throughout the
395 cytosol (Fig. 4f). The cells containing 2.9-3.4 μM FAM-Xpep-TAT (see Supplementary Fig. 5b
396 for the concentration calibration; in the following, we describe this concentration range as ≈3
397 μM for conciseness) were selected and the effects of these cytoplasmic peptides on the OR
398 homodimerization were examined. The results indicated that ≈3 μM FAM-peptide-TAT
399 significantly blocked the homo-dimerization (Fig. 4g; Table 1), consistent with the data
400 obtained using mGFP-Xpeps (Fig. 4c). The control FAM-Xpep-TATs (FAM-Dpep-TAT for KOR
401 and MOR and FAM-Kpep-TAT for DOR) did not affect the colocalization indexes. The effects
402 on colocalization durations were consistent with these results and with those obtained by
403 expressing mGFP-Xpeps (Fig. 4h; compare with Fig. 4d; Table 1).
404 The Xpep concentrations required for blocking homodimer formation might appear quite
405 high (≈3 μM), compared with the ≈30-nM-level dissociation constants of various agonists and
406 antagonists for ORs. However, note that the latter is the value for simple binding of the
407 ligand to the receptor, whereas the former addresses the extremely efficient dimerization

408 propensities of membrane molecules in the two-dimensional (2D) PM. The efficiency of
409 dimerization in 2D space was previously found to be higher by a factor of 10^6 than that in 3D
410 space.[59]

411 The effects of the presence of ≈3 μM FAM-Xpep-TATs in the cytoplasm on the
412 homodimer K_D, k_{off}, and k_{on} values are summarized in Fig. 4i. In addition to K_D and k_{on}, FAM-
413 Xpep-TATs increased k_{off} (enhanced dimer dissociation), indicating that the OR
414 homodimerization cannot be described by simple first-order kinetics (simple binding reaction
415 at the C-terminal domains), perhaps due to the conformational changes of the C-terminal
416 domains induced by the peptide binding and/or to the presence of weaker secondary binding
417 sites such as TM domains (Fig. 5, which will be discussed later). Nevertheless, we think the
418 present simplified approach is useful as the starting point for quantitative understanding of
419 the dynamic equilibrium between OR homodimers and monomers.
420

421 **Agonists modulate monomer-dimer interconversions, and FAM-Xpep-TAT peptides**
422 **reduce their effects**

423 The addition of representative agonists, U-50488 for KOR, [D-Ala^2, N-Me-Phe^4, Gly^5-ol]-
424 enkephalin acetate salt (DAMGO) for MOR, and SNC-80 for DOR, at 0.2 μM (a concentration
425 sufficient to ligate virtually all OR molecules) affected the homodimerizations of the three ORs
426 differently (observed during 2-5 min after agonist addition rather than after longer incubation
427 because these agonists induce OR internalizations, which become evident after 5 min;
428 discussed later in this report). The agonist-bound KOR exhibited less homodimerization (lower
429 colocalization index), whereas the agonist-bound MOR and DOR exhibited more
430 homodimerization (Fig. 4g and Table 1), although these results might vary depending on the
431 particular agonist.[9, 14] For example, the DOR agonists, DADLE, DSLET, and DPDPE, were
432 previously found to induce fewer homodimers,[9] but in the present research, another DOR
433 agonist SNC-80 was found to increase the homodimer fraction, suggesting that the
434 dimerization propensity depends on each agonist. We only examined one agonist for each OR
435 subtype, because an extensive examination of the agonist effects on OR homodimerization is
436 beyond the scope of the present work.

437 The colocalization indexes of the agonist-bound ORs were reduced by the addition of
438 FAM-Xpep-TAT for all ORs, but in different ways depending on the OR type (Fig. 4g). The
439 colocalization index of the agonist-bound KOR, which exhibited a smaller index as compared
440 with that of non-ligated KOR, was further reduced by the presence of FAM-Kpep-TAT
441 (although with no statistical significance). The colocalization index of the agonist-bound MOR
442 was reduced in the presence of FAM-Mpep-TAT to a level near that for MOR with the FAM-
443 Mpep-TAT without the agonist. The colocalization index of the agonist-bound DOR was
444 reduced in the presence of FAM-Dpep-TAT, but was still greater than that of wild-type DOR in
445 the absence of the agonist. The reason for this higher tendency to form homodimers even in
446 the presence of FAM-Dpep-TAT is unknown, but we propose that the agonist-induced
447 conformational changes enhanced the interaction in the TM domains, because DOR
448 homodimerization also involves TM-domain interactions (see Fig. 5, which will be discussed in
449 the next subsection). The effects of the agonists and homodimer blocker peptides on the
450 colocalization *durations* were consistent with the colocalization index data (Fig. 4h), and the
451 agonists' effects on the homodimer K_D, k_{off}, and k_{on}, as well as the percentages of OR
452 protomers existing as homodimers are summarized in Fig. 4i. The actual copy numbers of OR
453 protomers existing as monomers and homodimers at various total numbers of OR molecules
454 in the entire PM in a cell are summarized in Supplementary Table 2.
455

456 **MOR's transmembrane domain 1 ($TM1^{MOR}$) is involved in MOR homodimerization**
457 **with less specificity**

458 Specific C-terminal cytoplasmic domain deletions/mutations and the addition of peptides with
459 the same amino acid sequences as the deleted sequences greatly reduced the OR
460 homodimers' colocalization indexes, but never to be compatible with 1 found for rotated
461 overlays or 1.1 found for the monomer control molecule TM^{LDLR} (Fig. 2a). Therefore, we
462 considered the existence of other OR sites for homodimer formation. Since the involvement of
463 transmembrane domains in OR homo- and hetero-dimerization has been proposed,[20, 21, 26, 49,
464 50, 52, 53] and the first OR transmembrane domain (TM1) is often mentioned in the literature,[26,
465 49, 50] we examined the involvement of MOR's TM1 domain ($TM1^{MOR}$) in MOR homodimerization
466 (Fig. 5a).

467 Colocalization indexes indicated that $TM1^{MOR}$ interacts with another $TM1^{MOR}$ and MOR, as
468 well as, importantly, with DOR (Fig. 5b; the fluorescent spot number densities of the two
469 molecules in the PM were always adjusted to ≈1 spot/μm^2, and thus the number ratio was
470 approximately 1:1). These results suggest that $TM1^{MOR}$ is involved in MOR homodimerization
471 by the $TM1^{MOR}$-$TM1^{MOR}$ interaction, as well as, surprisingly, in MOR-DOR heterodimerization.
472 These results are supported by the observation of the colocalization *durations* (Fig. 5c).
473 In contrast, in the homodimer blocking experiments where $TM1^{MOR}$ is expressed ≈10x
474 more than MOR or DOR (Fig. 5d), $TM1^{MOR}$ moderately suppressed both MOR and DOR
475 homodimers (positive controls, Mpep and Dpep, respectively: negative controls, TM^{LDLR} = the
476 TM domain of LDL receptor and Xpeps specific for different OR homodimers; Fig. 5e).
477 Particularly, $TM1^{MOR}$ reduced both MOR and DOR homodimers, whereas Mpep reduced MOR
478 homodimers and not DOR homodimers and Dpep reduced DOR homodimers and not MOR
479 homodimers. Taken together, we conclude that the interaction specificity of $TM1^{MOR}$ is limited
480 as shown from its ability to interact with both MOR and DOR (Fig. 5b, e). The results showing
481 that $TM1^{MOR}$ suppresses both MOR-MOR and DOR-DOR homodimerization indicate that
482 $TM1^{MOR}$ is involved in both MOR homodimerization and MOR-DOR heterodimerization (also
483 refer to Figure 5C in the companion paper for the involvement of $TM1^{MOR}$ for MOR-DOR
484 heterodimerization). These results further indicate that $TM1^{MOR}$ might not be useful as a
485 specific blocker for MOR homodimerization or MOR-DOR heterodimerization.
486
487 **No major effects of Xpeps on the agonist-induced OR internalization**
488 We specifically blocked OR homodimers by the addition of Xpeps (FAM-Xpep-TATs), and
489 examined the effects on the agonist-induced OR internalization. Since all experiments were
490 performed at expression levels of ≈1 OR spot/μm^2, the percentages of the OR protomers
491 existing as homodimers are 10-21% without any addition, 3.2-4.4% after the addition of
492 FAM-Xpep-TATs, and 10-18% after the agonist addition, which is decreased to 2.9-8.6% after
493 the further addition of FAM-Xpep-TATs (see the column of 1 copy/μm^2 in Fig. 4i).
494 OR internalization might be involved in opioid side effects and tolerance development.
495 Here, it was monitored by using the membrane-*im*permeable fluorescence quencher, Mn(III)
496 meso-tetra(4-sulfonatophenyl)porphine (Mn^{3+}-TSP). This quencher only suppresses

497 fluorescence emission from the SNAP-Surface 549 dye on the SNAPf-OR on the cell surface,
498 but not that in the cytoplasm.[60]
499 Accordingly, by subtracting the signal intensity after the quencher addition from that
500 before the addition, we evaluated the percentages of OR molecules remaining in the PM (Fig.
501 6a and Supplementary Fig. 6).
502 The time courses of the decrease in the numbers of ORs remaining in the PM during 35
503 min (due to their internalization) were examined in both the presence and absence of 0.2 μM
504 agonists and ≈3 μM Xpeps in the cytoplasm (Fig. 6b; Table 1 and Supplementary Table 1). All
505 the time-course data obtained under various conditions could be fitted with a single
506 exponential function plus a constant. The constant provides the OR fraction whose
507 internalization is undetectable by the 35-min observations, and the exponential decay
508 constant provides the residency lifetime in the PM for the OR component whose
509 internalization was detectable by this observation scheme (Table 1 and Supplementary Table
510 1). Without agonist, the three ORs all exhibited non-internalized fractions in the range of 91-
511 97% (for an observation period of 35 min). The internalized molecules found during the 35-
512 min observations showed characteristic dwell lifetimes (inverse of internalization rates)
513 between 24 and 45 min. The homodimer-blocking peptides, FAM-Xpep-TATs, did not
514 significantly affect the OR internalization (Fig. 6b and Table 1).
515 The addition of agonists employed in this investigation greatly increased the fractions of
516 detectable internalizations and the internalization rates for all three ORs (Fig. 6b and Table
517 1), although it decreases the percentages of KOR protomers existing as homodimers from 21
518 to 10% but increases the percentages from 11 to 18% and 10 to 17% for MOR and DOR,
519 respectively (Fig. 4i). The FAM-Xpep-TATs reduced the homodimer percentages to 2.9, 3.3,
520 and 8.6% for the engaged KOR, MOR, and DOR, respectively (Fig. 4i). The internalization
521 observations indicated that for the engaged KOR, the addition of FAM-Kpep-TAT induced only
522 slightly faster internalization, whereas for the engaged MOR and DOR, no differences in
523 internalization were detectable after the addition of FAM-Mpep-TAT and FAM-Dpep-TAT (Fig.
524 6b and Table 1).
525 The lack of effect (or only the slight effect) of FAM-Xpep-TATs on the agonist-induced
526 OR internalization is probably because monomers and homodimers are internalized at about

527 the same rate. This might be induced if the internalization rate of homodimers as an
528 internalization unit (two protomers together as a homodimer) might become about half of
529 that of monomers or if the complex processes involving GRK and β-arrestin 2[29, 61, 62, 63] might
530 remove the ORs bound by these proteins from the monomer-dimer equilibrium in the bulk
531 PM.[87-90] However, due caution in the interpretation of these data is required because the
532 Xpep-bound C-terminal domain might inhibit or enhance the interaction with GRK and β-
533 arrestin 2 (for the Gqi5 binding, see the next subsection).
534 In addition to CHO-K1 cells, T24 cells were employed for these experiments because
535 the expression level of β2-arrestin in T24 cells is higher than that in CHO-K1 cells,[64] and thus
536 T24 cells might undergo more active internalization. However, T24 cells exhibited
537 internalization behaviors quite similar to those of CHO-K1 cells (Fig. 6b; Supplementary
538 Tables 1 and 3).
539
540 **Xpeps modulate KOR and DOR signals**
541 The agonist-induced signal downstream from the OR was examined by a widely used method
542 for Gi-coupled GPCRs, employing the artificial G protein Gqi5 (Fig. 6c-6e; refer to the caption
543 to Supplementary Fig. 1a and Methods).[65, 66, 67] The addition of the homodimer-blocking FAM-
544 Xpep-TATs alone (thus the monomerization of ORs alone) did not induce any detectable Ca^{2+}
545 mobilization (Fig. 6f and Table 1). Meanwhile, the respective agonists triggered Ca^{2+}
546 mobilization. The effects of the homodimer-blocking peptides on the agonist-induced Ca^{2+}
547 mobilization were complex (both FAM-Xpep-TATs and mGFP-Xpeps produced similar effects
548 for all three ORs). In cells expressing KOR, MOR, or DOR, the homodimer-blocking peptides
549 (OR monomerization) enhanced, did not affect, and reduced the agonist-induced Ca^{2+}
550 mobilization, respectively (Fig. 6f and Table 1). These results indicate that KOR and DOR
551 monomers trigger higher and lower signals than their respective homodimers, whereas MOR
552 monomers and homodimers induce the downstream signals at similar levels (without
553 influencing the agonist-induced internalization of all ORs; Fig. 6b). In short, homodimerization
554 suppresses the ligand-induced signaling of KOR and enhances the ligand-induced signaling of
555 DOR.

556 It is possible that these results might be induced by the interfering effect of the bound
557 peptide on the binding of Gqi5 to ORs (Gqi5's binding site to ORs is the same as the original
558 Gαi) because the Gi binding to class A GPCRs involves various intracellular domains.[62, 63, 68, 69,
559 70, 71] However, since the Halo-tag protein bound to the C-termini of ORs do not affect OR-
560 induced Ca^{2+} responses (Supplementary Fig. 1b of the companion paper) and since the
561 peptide binding induces distinct effects on the three ORs, we think it likely that the effect of
562 homodimer blocking peptides on the agonist-induced Ca^{2+} signal can be interpreted based on
563 its effect on OR monomerization.
564 Furthermore, these results suggest that the homodimer-blocking peptide-TATs could be
565 used as reagents (drugs) to enhance or suppress the agonist-induced G-protein-biased
566 cellular responses for KOR and DOR, respectively, without affecting their internalization (Fig.
567 6b). However, note that these results are correct only for the employed agonists, and the
568 results would be agonist dependent.
569

570 # Discussion

571 For the first time, the three critical parameters describing the homodimer-monomer dynamic
572 equilibrium (K_D, k_{on}, and k_{off}) have been determined for the OR. This was done for the three
573 classical ORs before and after the addition of a representative agonist for each OR (Fig. 2b
574 and 4i). The results unequivocally demonstrated that the three classical ORs all form transient
575 metastable homodimers at physiological expression levels (0.3-10 copies/μm^2) at 37°C, and
576 predicting that 3.4-59% of OR protomers would exist as homodimers in various tissues both
577 before and after the agonist binding (Fig. 2d). Accurate evaluation of the dimer dissociation
578 rate constant (k_{off}) in the live-cell PM using single-molecule colocalization data became
579 possible by developing a theory (Supplementary Note 1), and the dimer-monomer
580 dissociation equilibrium constant (K_D) could be obtained much more readily compared with
581 the method we developed previously.[37] These theories/methods enabled accurate
582 quantitative evaluations of k_{off} and K_D, and would be applicable to evaluate the dimerization
583 kinetics and equilibrium of any membrane molecules, as exemplified by their application to
584 OR heterodimerization described in the companion paper.[38] Accordingly, they represent major
585 developments for studies of molecular interactions in the PM in general.

586 A previous single-molecule imaging study of neurotensin receptor 1, a GPCR, in
587 reconstituted membranes containing only this receptor and a phospholipid revealed that it
588 forms homodimers. This result demonstrated that neurotensin receptor 1 homodimerization
589 occurs without the involvement of any other proteins[21] (however, see[14]), and suggested that
590 ORs might also form homodimers in a similar manner.

591 Importantly, all of these homodimers are forming and dispersing continually, with
592 lifetimes shorter than 0.2 s at 37°C (Fig. 1d). When the homodimers dissociate into
593 monomers, they will again form homodimers with the same and other partner molecules.
594 Longer homodimer lifetimes on the order of 0.5-2 s or even 15 s have been reported, but
595 they were observed at lower temperatures such as RT and 20°C.[33, 34, 35] How the limited
596 dimer fractions and lifetimes modulate the downstream signaling and internalization is
597 extensively discussed in the companion paper (refer to Figure 7C and related main text in the
598 companion paper).

599 Specific 9-26 residue amino-acid sequences in the near-C-terminal cytoplasmic domains,
600 which lack sequence similarities among the three ORs, are involved in the distinct
601 homodimerizations of all three classical ORs (Fig. 3b, c, and 4), and do not participate in
602 heterodimerization (Fig. 2a and 3a in the companion paper). In addition to localized
603 electrostatic interactions between charged amino acid residues, the overall structures of the
604 cytoplasmic C-terminal domains, and particularly the intrinsically disordered structures of the
605 C-terminal regions, might be important for homodimerization.[56] The enhancement of
606 homodimerization by the intrinsically disordered region might not be due to liquid-liquid
607 phase separation, but rather to its ability to flexibly adopt various structures, bringing specific
608 binding sites into positions and orientations for optimal interactions.
609 In the literature on homo- and hetero-dimerization of GPCRs, including ORs, the TM
610 domains have been proposed or found to be responsible for homodimerization.[21, 26, 49, 50, 52, 53]
611 In the present study, we experimentally and directly confirmed this using $TM1^{MOR}$, but we
612 also found that $TM1^{MOR}$ binding to ORs is likely to be quite non-specific, as found by its
613 binding to DOR as well as MOR, and its suppressive effect on both DOR and MOR
614 homodimerization. Blocking of DOR homodimerization of $TM1^{MOR}$ suggests that it is also
615 involved in DOR-MOR heterodimerization. Furthermore, we found that Xpeps failed to reduce
616 the OR homo-colocalization indexes to the level of a monomer control molecule TM^{LDLR}.
617 Therefore, we propose that TM-TM interactions enhance both the homo- and hetero-
618 dimerizations of ORs in less specific manners, whereas the cytoplasmic C-terminal domain
619 interactions provide the specificities for OR homodimerization.
620 To the best of our knowledge, the Xpep-TATs developed here are the first peptide-
621 based reagents that specifically reduce GPCR homodimerization. These homodimer-blocking
622 peptides can become important tools to dissect the functions of OR monomers and
623 homodimers. The use of the Xpeps revealed that DOR and KOR homodimers, but not MOR
624 homodimers, induce G-protein-dependent signals differently from their respective monomers
625 (Fig. 6f), although both monomers and homodimers are internalized at the same rate before
626 and after agonist addition (Fig. 6b). These results suggest that the C-terminal domain
627 conformations of the DOR and KOR homodimers might undergo allosteric changes upon
628 homodimerization, affecting their G-protein-based signaling. The possibility of the

involvement of allosteric conformational changes of ORs upon dimerization will be further discussed in the companion paper (allosteric effects might be more important for DOR-MOR heterodimers).

These homodimer blocking peptides could become the basis for designing modulators and potentiators in opioid therapy to enhance the efficacy and suppress side effects such as tolerance development, particularly for the opioids targeting KOR and DOR. The development of agonists for favorable biased signaling is important,[72, 73, 74, 75] but the modulation of the OR homodimerization would provide another means to produce biased signaling. Since the Xpep-TATs are soluble and yet membrane-permeable (Fig. 4e-h) and thus they are likely to pass the blood-brain barrier, they could be readily delivered via intravenous injections or nasal sprays. In addition, Xpep-TATs would not compete with agonist binding because they bind to the cytoplasmic C-terminal domains. Taken together, our findings reported here have greatly extended our knowledge of ORs' metastable homodimers and their formation mechanisms and functions, which can inform novel GPCR drug development strategies of modulating homodimerization.

Figures

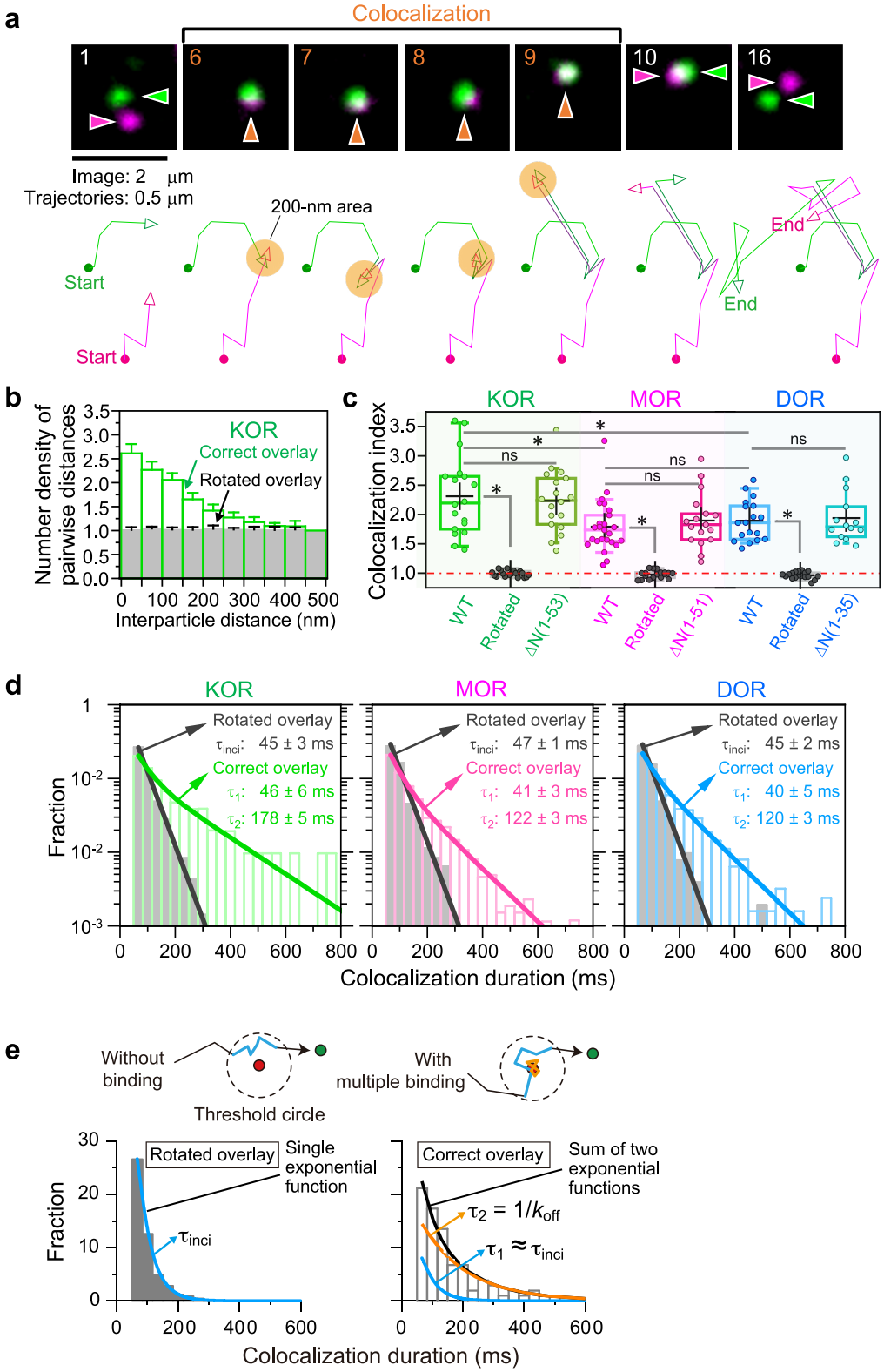

Fig. 1: ORs in the PM form metastable homodimers with lifetimes of 120~150 ms, without involving the N-terminal extracellular domain.

a Typical image sequence of simultaneous two-color single fluorescent molecule observations, showing transient homo-colocalization and co-diffusion of single molecules of SNAPf-KOR tagged with SNAP-CF 660R (magenta) and SNAP-Surface 549 (green), with their trajectories.

b PCCFs for the SNAPf-KOR spots (mean ± SEM after area normalization; 18 movies). Green and grey bars indicate the results of the correct and 180°-rotated overlays of the simultaneously observed magenta and green images. The colocalization index is defined as the mean of PCCF values for 0-100 nm divided by the mean of PCCF values for 400-500 nm (see Supplementary Fig. 2c-e).

c Colocalization indexes showing the homo-colocalizations of three ORs and OR mutants with deletions of the N-terminal extracellular domains.

Throughout this study, we employ the following conventions: for the box plots, horizontal bars, crosses, boxes, and whiskers indicate median values, mean values, interquartile ranges (25–75%), and 10-90% ranges, respectively; for the bar graphs and tables, mean ± SEM values are provided; and for the statistical analyses, * and ns represent significant ($p < 0.05$) and non-significant ($p \geq 0.05$) differences, respectively. The p values were obtained by Tukey's multiple comparison test, except the Brunner-Munzel test used for colocalization lifetimes. All of the quantitative results are summarized in Table 1 and their statistical parameters (sample size n and p values) are provided in Supplementary Table 1.

d Histograms showing the distributions of colocalization *durations* for correct and rotated overlays. The control histograms for rotated overlays (grey) were fitted by single exponential functions (black), providing the lifetime of the incidental overlap events (τ_{inci}). The histograms for correct overlays (colors) were fitted by the sum of two exponential functions: The faster decay time (τ_1) was close to τ_{inci}, and the slower decay time provided the true homodimer lifetime (τ_2; see Supplementary Note 1 for the theory). The homodimer lifetimes, after correction for the trackable duration lifetimes of the two fluorescent probes, are shown in the boxes (summarized in Table 1).

e The method to determine the true dissociation rate constant (k_{off}), considering the multiple binding events during an observed colocalization duration. See Supplementary Note 1.

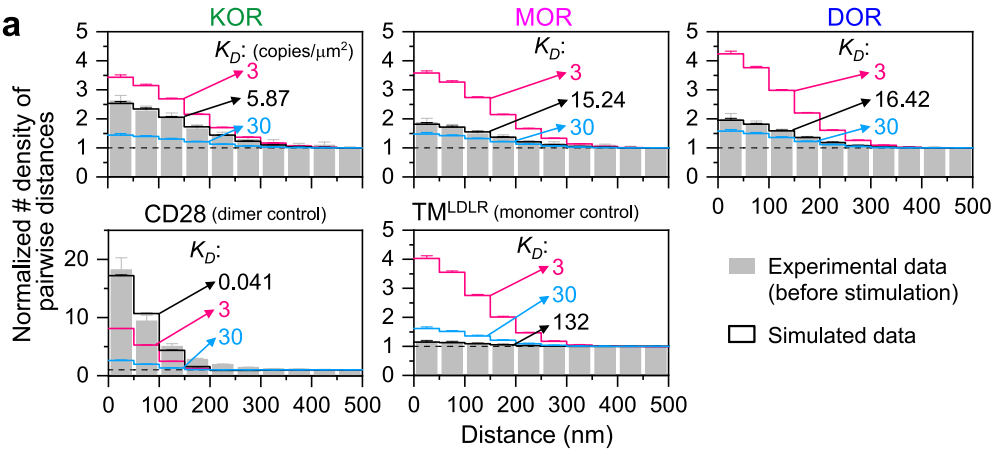

b

ORs	K_D (copies/μm²)	k_{off} (s⁻¹)	k_{on} (μm²/copies/s)	Predicted %OR protomers existing as dimers at different expression levels (copies/μm²)				
				0.3	1	3	10	30
KOR	5.87 ± 0.56	6.71 ± 1.17	1.14 ± 0.23	8.6	21	39	59	73
MOR	15.24 ± 1.54	8.47 ± 0.86	0.56 ± 0.08	3.7	11	23	43	61
DOR	16.42 ± 0.53	8.00 ± 0.96	0.49 ± 0.06	3.4	10	22	42	60
CD28	0.041 ± 0.072	N.D.	N.D.					
TM^LDLR	132 ± 21	N.D.	N.D.					

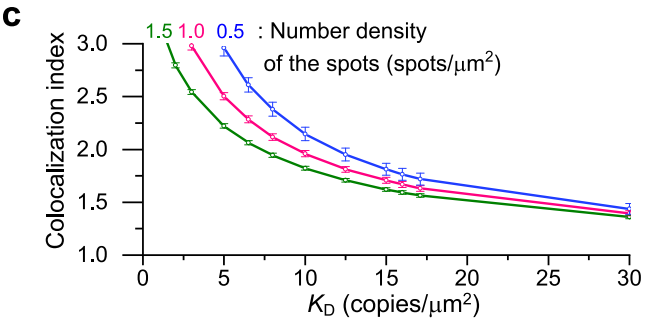

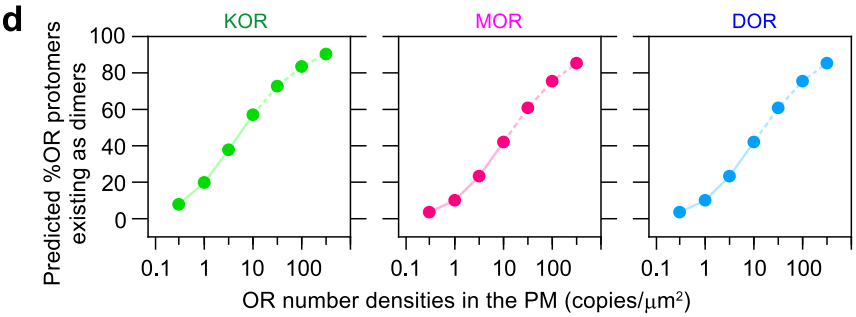

Fig. 2: Dynamic OR homodimer-monomer equilibrium constants (K_Ds) and homodimer formation and dissociation rate constants (k_{on} and k_{off}, respectively), providing the %protomers existing as dimers as a function of the expression level.

a Experimental PCCFs for KOR, MOR, DOR, CD28, and TM^{LDLR} (the PCCF for KOR is the same as that shown in Fig. 1c) fitted with theoretical PCCFs (Eq. 24) in Supplementary Note 2; the total numbers of fluorescent spots, sN_{TA} and sN_{TB}, were determined from experiments; labeling efficiency = 0.7 [Supplementary Fig. 1e]) using K_D and σ as fitting parameters. CD28 and TM^{LDLR} were dimer and monomer references, respectively. The black lines indicate the best-fit functions, and their K_D values are shown. The PCCFs with K_D values of 3 and 30 are also shown for comparison.

b Summary of K_D, k_{off} and k_{on} values for the three ORs without agonist, and also for CD28 and TM^{LDLR}. N.D.: not done. Predicted percentages of OR protomers existing as dimers at various expression levels calculated from the K_Ds are also shown. Physiological expression levels found in the literature (1-10 copies/μm^2) are highlighted by a pink background (see the main text).

c Colocalization index is simply related to K_D, if the labeling efficiency, the precision of single-molecule localization plus image overlaying, and the number density of fluorescent molecules in each movie were the same (0.7, 140 nm, and 0.5, 1, or 1.5 fluorescent spots/μm^2, respectively). K_D can be roughly estimated from the colocalization index using these curves.

d Predicted percentages of OR protomers existing as dimers, plotted as a function of expression levels (without agonist). The curves indicate the mathematical functions calculated from the K_D values, and solid curves are used for physiological expression levels found in the literature (0.32-10 copies/μm^2). Tick marks between the exact digits represent ≈3.16x ($10^{0.5}$x) of the smaller digit.

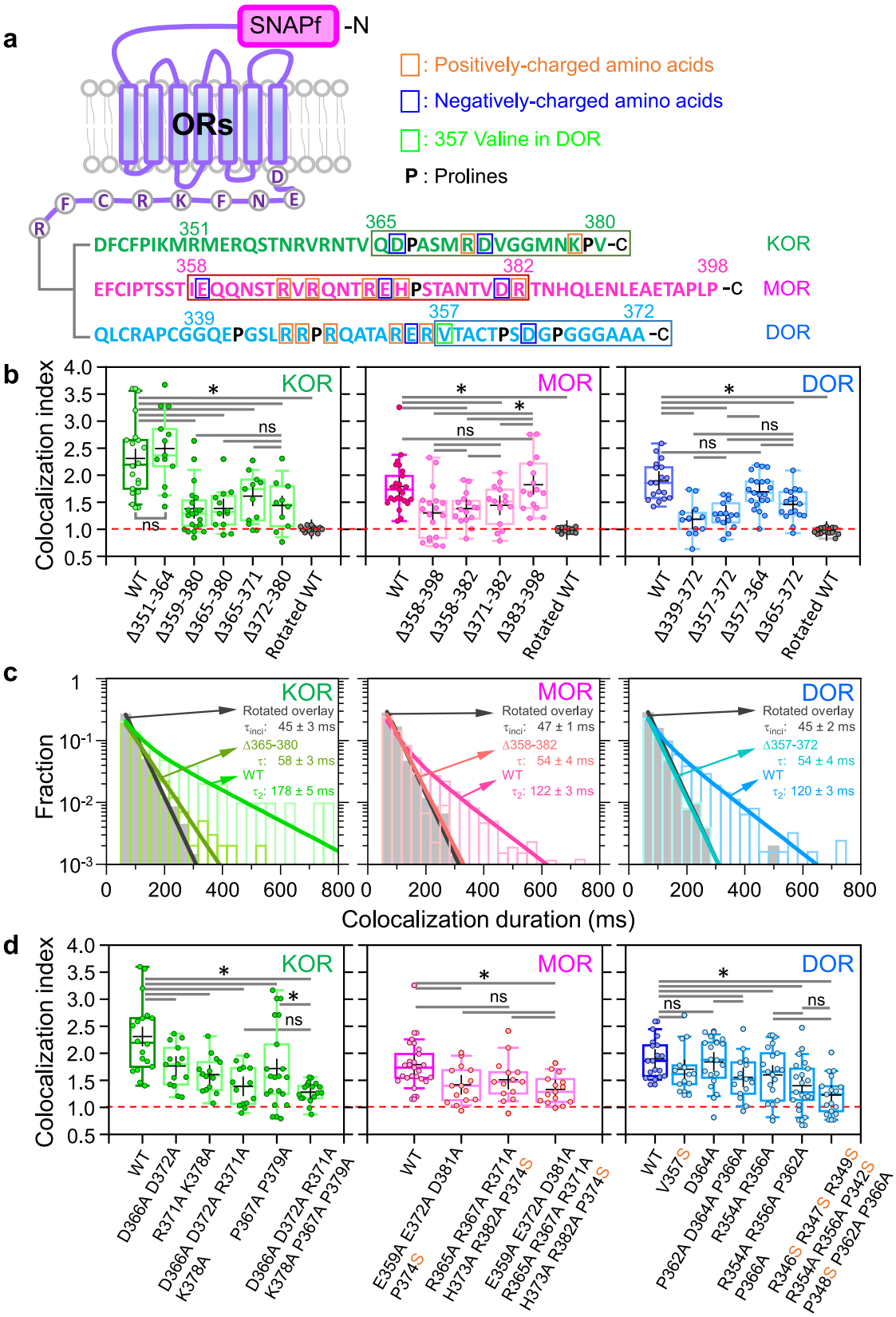

Fig. 3: C-terminal cytoplasmic domains are predominantly responsible for OR homodimerization.

715 **a** Schematic figure showing the amino-acid sequences of the C-terminal cytoplasmic domains
716 of the three ORs. The sequences surrounded by rectangles were extensively examined for
717 their involvement in OR homodimerization.
718 **b** Colocalization indexes for WT and various C-terminal cytoplasmic deletion mutants,
719 showing that KOR aa 365-380, MOR aa 358-382, and DOR aa 357-372, with very low amino-
720 acid homologies, are critical for homodimerization.
721 **c** Histograms showing the distributions of colocalization *durations* for the C-terminal
722 cytoplasmic deletion mutants, KOR(Δ365-380), MOR(Δ358-382), and DOR(Δ357-372) (only
723 the results of correct overlays). WT-OR data are reproduced for comparison (for both correct
724 and rotated overlays; Fig. 1d). Deletion mutants exhibited distributions that could be fitted by
725 single exponential functions, and their decay time constants τs (after correction for the
726 trackable duration lifetimes of the two fluorescent probes) are indicated in the boxes.
727 **d** The colocalization indexes of various C-terminal point mutants, indicating that the charged
728 groups and prolines in the C-terminal cytoplasmic domains play important roles in OR
729 homodimerization.
730

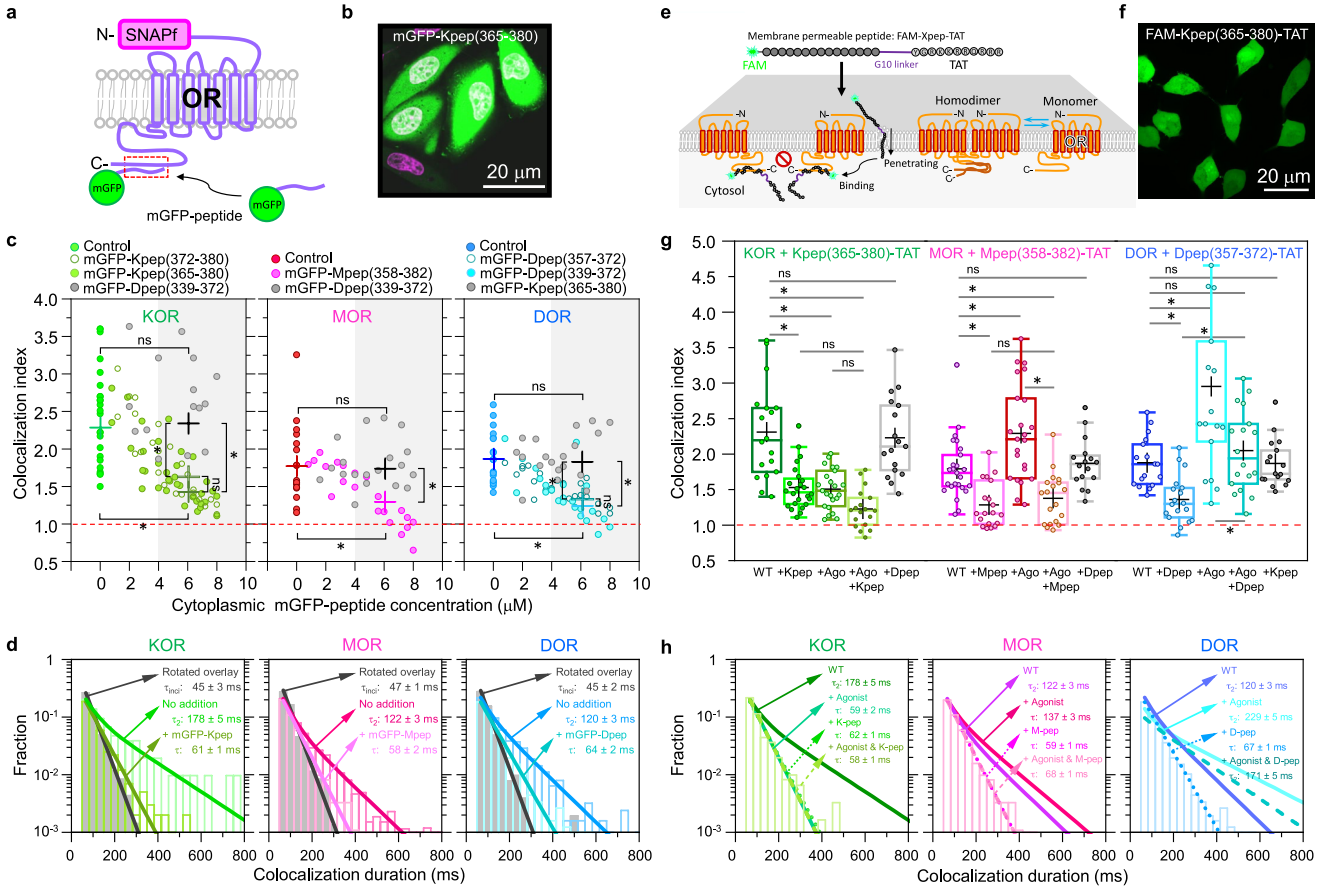

i

ORs	Agonist	Xpep	K_D (copies/µm²)	k_{off} (s⁻¹)	k_{on} (µm²/copies/s)	Predicted %OR protomers existing as dimers at different expression levels (copies/µm²)				
						0.3	1	3	10	30
KOR	–	–	5.87 ± 0.56	6.71 ± 1.17	1.14 ± 0.23	8.6	21	39	59	73
	–	+	58.02 ± 6.71	16.13 ± 0.26	0.28 ± 0.03	1.0	3.2	8.6	21	39
	+	–	15.81 ± 1.36	17.86 ± 0.32	1.13 ± 0.10	3.5	10	23	42	60
	+	+	65.05 ± 16.00	17.24 ± 0.30	0.27 ± 0.07	0.9	2.9	7.8	20	37
MOR	–	–	15.24 ± 1.54	8.47 ± 0.86	0.56 ± 0.08	3.7	11	23	43	61
	–	+	45.51 ± 7.92	16.95 ± 0.29	0.37 ± 0.07	1.3	4.0	11	25	43
	+	–	8.34 ± 0.58	5.35 ± 1.69	0.64 ± 0.21	6.8	18	34	54	70
	+	+	56.44 ± 8.15	14.71 ± 0.22	0.26 ± 0.04	1.0	3.3	8.8	22	39
DOR	–	–	16.42 ± 0.53	8.00 ± 0.96	0.49 ± 0.06	3.4	10	22	42	60
	–	+	41.21 ± 3.26	14.93 ± 0.22	0.36 ± 0.03	1.4	4.4	11	26	45
	+	–	7.69 ± 0.36	3.62 ± 0.25	0.47 ± 0.04	6.3	17	33	53	69
	+	+	19.56 ± 1.80	5.88 ± 0.17	0.30 ± 0.03	2.9	8.6	20	39	57

Fig. 4: Specific C-terminal-domain peptides suppress OR homodimerization.

a Schematic figure showing the experimental design to examine the effects of mGFP-Xpeps expressed in the cell on OR homodimerization.

b Representative confocal image of CHO-K1 cells transfected with cDNAs encoding SNAPf-KOR (not visible here; only visible by single-molecule imaging conditions) and mGFP-Kpep (green), co-stained with the Live 650 Nuclear Stain (magenta; white nuclei indicate the

738 entrance of mGFP-Kpep into the nuclei, whereas a magenta nucleus indicates the cell without
739 mGFP-Kpep expression).
740 **c** The OR homo-colocalization index in each cell tends to decrease with an increase of the
741 mGFP-Xpep concentration in the cytoplasm. The + keys at x = 0 and 6 μM mGFP-Xpep
742 indicate the mean value of the colocalization indexes without mGFP-Xpep expression and that
743 averaged over all the data points in the range of 3.8-7.8 μM mGFP-Xpep, respectively.
744 Significant reductions of the colocalization indexes in the presence of the mGFP-Xpeps, but
745 not the control mGFP-peptides, were found for all three ORs (Table 1).
746 **d** Histograms showing the *duration* distributions of transient homodimers of SNAPf-ORs in
747 cells co-expressing 3.8-7.8 μM mGFP-Xpeps (only the results of correct overlays; the value for
748 each bin is the mean of 18 cells), compared with those without co-expression (the same as
749 those shown in Fig. 1d; for both correct and rotated overlays). For further details of these
750 graphs, see the caption to Fig. 3c.
751 **e** Schematic figure showing the experimental design to examine the effect of the FAM-Xpep-
752 TATs incorporated in the cell on OR homodimerization.
753 **f** Representative confocal image of CHO-K1 cells containing an average of 3.4 μM FAM-Kpep-
754 TAT in the cytoplasm.
755 **g, h** Agonist addition (0.2 μM) suppressed KOR homodimerization, but enhanced the
756 homodimerization of MOR and DOR (colocalization indexes in **g** and durations of
757 colocalization events in **h**). The presence of ≈3 μM FAM-Xpep-TAT in the cytoplasm
758 suppressed homodimerization both before and 2-5 min after the agonist addition.
759 (**i**) Summary of K_D (homodimer-monomer equilibrium constant), k_{off} (dimer dissociation rate
760 constant), and k_{on} (dimer formation rate constant) for three ORs in the presence and absence
761 of ≈3 μM FAM-Xpep-TAT in the cytoplasm, both before and 2-5 min after the addition of
762 agonists. Predicted percentages of OR protomers existing as dimers at various expression
763 levels calculated from the K_Ds are also shown. Physiological expression levels found in the
764 literature are highlighted by a pink background (see the main text).
765

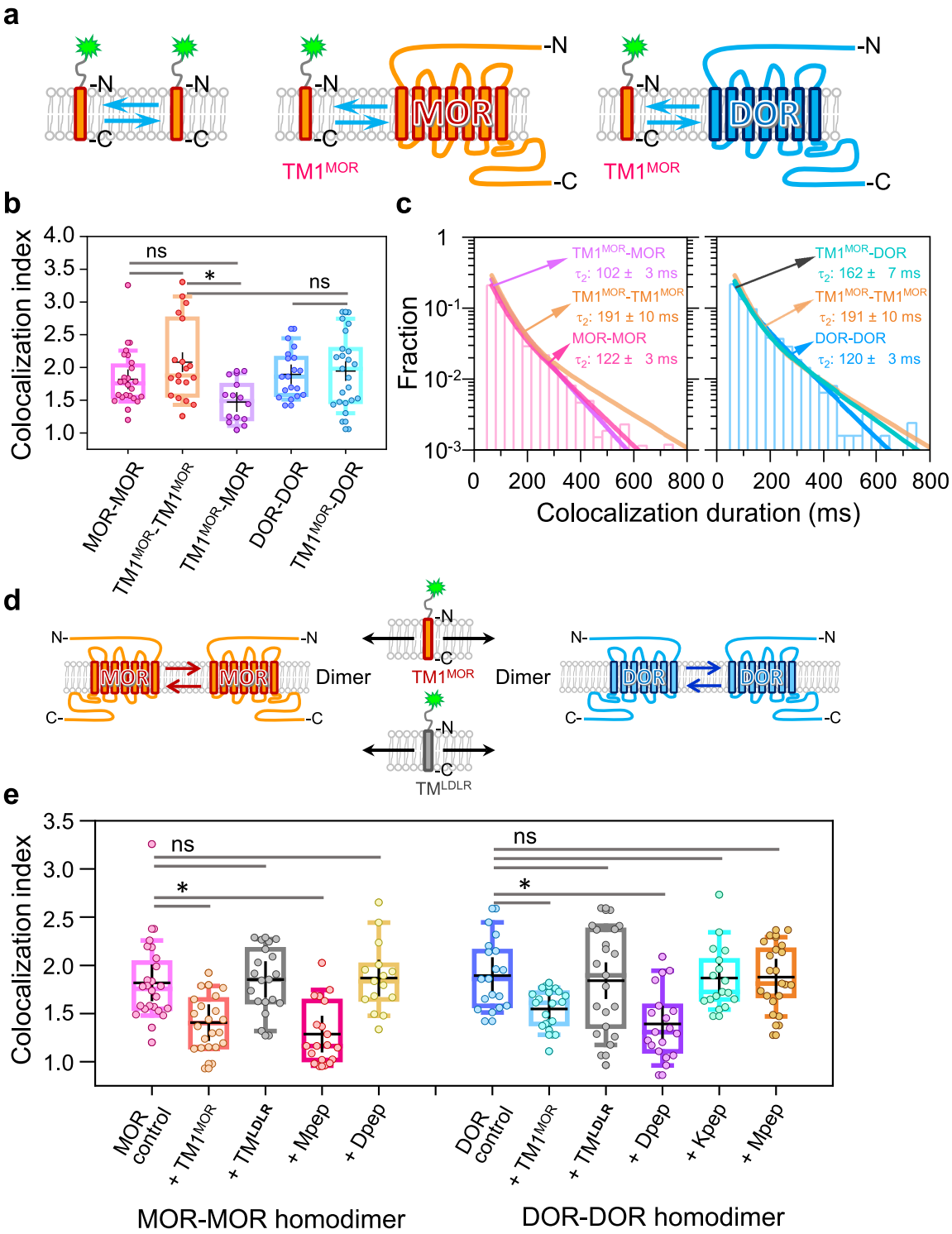

Fig. 5: TM1^{MOR} suppresses both MOR and DOR homodimerization.

a Schematic figure showing the experimental design for examining the interaction (binding) of TM1^{MOR} with itself, MOR, and DOR.

770 **b, c** Colocalization indexes (**b**) and distributions of colocalization durations (**c**) showing that
771 $TM1^{MOR}$ forms metastable dimers with both MOR and DOR, suggesting that $TM1^{MOR}$ might be
772 involved in MOR-MOR homodimerization as well as MOR-DOR heterodimerization (see Figure
773 5 in the companion paper.[38]
774 **d** Schematic figure showing the experimental design for examining whether $TM1^{MOR}$ can
775 suppress homodimerizations of MOR and DOR.
776 **e** $TM1^{MOR}$ suppresses both MOR and DOR homodimerization, whereas Mpep and Dpep
777 specifically suppress MOR or DOR homodimerization, respectively.
778

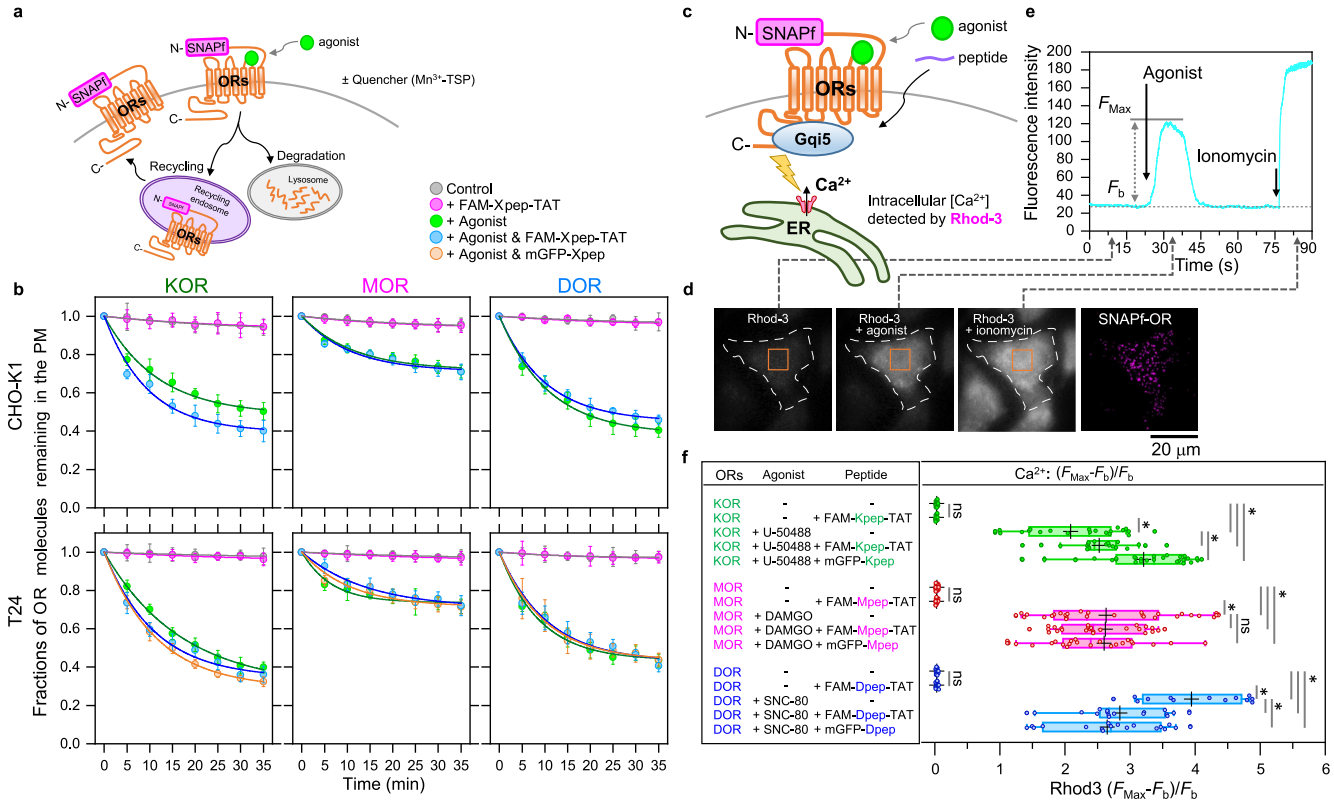

Fig. 6: Xpeps hardly affect OR internalization in both the presence and absence of the agonist, whereas they enhanced, did not affect, or reduced the Ca^{2+} mobilization induced by the KOR, MOR, and DOR agonists, respectively.

a Schematic figure showing the experimental design for observing the internalization of OR (with possible recycling). Also see Supplementary Fig. 6**.**

b Time-dependent decreases of SNAPf-ORs on the PM due to their internalizations in CHO-K1 cells (top) and T24 cells (bottom) (mean ± SEM; 10 cells for each condition), before and after the addition of 0.2 μM agonist in the presence and absence of ≈3 μM FAM-Xpep-TATs and ≈6 μM mGFP-Xpeps in the cytoplasm. Photobleaching of the fluorescent probe is negligible because only one frame was recorded every 5 min. The time courses could be operationally fitted by single exponential functions, $y = C*\exp(-t/\tau_0) + (1-C)$, providing the fractions of OR molecules with detectable (C) and non-detectable (1 - C) internalizations for the observations up to 35 min, as well as the residency times (τ_0) for the internalized component.

c Schematic figure showing the experimental design for observing the Ca^{2+} mobilization after the agonist stimulation. The Ca^{2+} mobilization was monitored by the Rhod-3 fluorescence intensity (see the caption to Supplementary Fig. 1a and Methods).

796 **d, e** Typical fluorescence images of Rhod-3 in cells (**d**; orange rectangles = ROI) and the
797 time-dependent changes of the Rhod-3 signal intensity in the ROI (**e**), showing the changes
798 in the cytosolic Ca^{2+} concentration after the agonist stimulation. Cells with similar expression
799 levels of ORs (≈1 fluorescent spot/μm^2) were selected.
800 **f** Ca^{2+} mobilization at 75 s after the agonist addition, parametrized by using $[F_{Max}-F_b]/F_b$ (see
801 **e**).
802

Table 1. Summary of the colocalization indexes, homodimer lifetimes, fractions and PM residency times of molecules with internalizations detectable by the 35-min observations, and Ca^{2+} mobilization parameter, $(F_{Max}-F_b)/F_b$, in the presence and absence of various modulators (0.2 μM agonists, ≈3 μM FAM-Xpep-TATs in the cytoplasm, and ≈6 μM mGFP-Xpeps in the cytoplasm). The agonists employed here were U-50488 for KOR, DAMGO for MOR, and SNC-80 for DOR.

ORs	Additions	Colocalization Index (Mean ± SEM)	Homodimer Lifetime (Mean ± SEM) (ms)	Fraction of internalized molecules (%)	PM residency time of internalized molecules (min)	Ca^{2+} $(F_{Max}-F_b)/F_b$
KOR	Control	2.30 ± 0.2	178 ± 5	8.4 ± 4.1	32.1 ± 23.8	0.04 ± 0.01
	+ FAM-pep-TAT	1.53 ± 0.1^{*,Na}	62 ± 1^{*,Na}	6.9 ± 2.4^{Nc,†}	26.2 ± 15.4^{Nc,†}	0.05 ± 0.01^{Nc,†}
	+ mGFP-pep	1.41 ± 0.1^{*,Na}	61 ± 1^{*,Na}	-	-	-
	+ Agonist	1.48 ± 0.1*	59 ± 2*	51.4 ± 2.7*	11.9 ± 1.7*	1.96 ± 0.32*
	+ Agonist + FAM-pep-TAT	1.23 ± 0.1*,†	58 ± 1^{*,Na}	60.5 ± 2.5*,†	9.6 ± 1.2^{*,Na}	2.46 ± 0.21*,†
	+ Agonist + mGFP-pep	1.17 ± 0.1*,†	54 ± 2^{*,Na}	-	-	3.11 ± 0.17*,†
MOR	Control	1.82 ± 0.1	122 ± 3	6.4 ± 1.9	25.8 ± 12.6	0.03 ± 0.01
	+ FAM-pep-TAT	1.38 ± 0.1*,†	59 ± 1*,†	6.3 ± 1.0^{Nc,†}	22.1 ± 4.1^{Nc,†}	0.04 ± 0.01^{Nc,†}
	+ mGFP-pep	1.32 ± 0.1*,†	58 ± 2*,†	-	-	-
	+ Agonist	2.18 ± 0.2*	137 ± 3*	28.1 ± 1.7*	11.3 ± 1.9*	2.80 ± 0.21*
	+ Agonist + FAM-pep-TAT	1.38 ± 0.1*,†	68 ± 1*,†	28.9 ± 2.0^{*,Na}	10.7 ± 2.1^{*,Na}	2.78 ± 0.22^{*,Na}
	+ Agonist + mGFP-pep	1.34 ± 0.1*,†	67 ± 3*,†	-	-	2.80 ± 0.24^{*,Na}
DOR	Control	1.89 ± 0.1	120 ± 3	4.5 ± 3.5	29.8 ± 37.4	0.05 ± 0.01
	+ FAM-pep-TAT	1.36 ± 0.1*,†	67 ± 1*,†	4.9 ± 2.5^{Nc,†}	26.2 ± 22.6^{Nc,†}	0.05 ± 0.01^{Nc,†}
	+ mGFP-pep	1.29 ± 0.1*,†	64 ± 2*,†	-	-	-
	+ Agonist	3.00 ± 0.3*	229 ± 5*	61.6 ± 1.7*	10.8 ± 0.9*	3.85 ± 0.23*
	+ Agonist + FAM-pep-TAT	2.08 ± 0.2*,†	171 ± 5*,†	55.0 ± 1.0*,†	10.1 ± 0.5^{*,Na}	2.84 ± 0.20*,†
	+ Agonist + mGFP-pep	2.00 ± 0.2*,†	168 ± 5^{Nc,†}	-	-	2.65 ± 0.22*,†

* $^{(Nc)}$: Significant (insignificant) difference from the value for "Control".

† $^{(Na)}$: Significant (insignificant) difference from the value for "+ Agonist".

814 # Methods

815 **cDNA construction**

816 All of the newly generated cDNA constructs and other constructs obtained from outside
817 sources, including gifts and constructs from commercial sources, were sequenced to examine
818 their exact DNA sequences. The cDNA encoding rat MOR tagged with GFP was a gift from Dr.
819 R. Schülz of the University of Münich, Germany.[76] The cDNA encoding rat KOR and DOR was
820 a gift from Dr. Hiroshi Takeshima of the Kyoto University.[77] The mCherry was a gift from Prof.
821 R. Y. Tsien of the University of California San Diego.[78] The cDNA encoding CD47 was a gift
822 from Eric C Brown of Genentech.[79] The cDNA encoding CD28 was a gift from Simon J Davis of
823 University of Oxford.[80] The cDNAs encoding SNAPf and mGFP (A206K) were obtained from
824 Promega and Clontech, respectively. To generate plasmids for expressing SNAPf-ORs in CHO-
825 K1 cells, the tag protein SNAPf was attached to the N-terminus of the ORs, an additional
826 signal sequence of interleukin 6 was attached to the N-terminus of the tag protein, and a 21
827 amino-acid linker (SGGGSGG x3) was inserted between the ORs and the tag protein. A Site-
828 Directed Mutagenesis Kit (New England Biolabs) was used to generate the cDNAs encoding
829 the OR point mutants.

830

831 **Cell culture, transfection, and microscope observations**

832 CHO-K1 cells (Dainippon Pharma) and T24 cells (gift from Prof. M. Sokabe of Nagoya
833 University),[81] confirmed free of mycoplasma contamination by MycoAlert (Lonza), were
834 routinely cultured in Ham's Nutrient Mixture F12 (Sigma-Aldrich) supplemented with 10%
835 (v/v) fetal bovine serum (FBS, Life Technologies), 100 units/ml penicillin, and 0.1 mg/ml
836 streptomycin, at 37°C under a 5% CO_2 atmosphere in the incubator. Transfection of CHO-K1
837 cells with the cDNAs of interest was performed by electroporation, according to the
838 manufacturer's instructions (4D-Nucleofector, Lonza; SF Cell Line solution and program CHO-
839 K1 for CHO-K1 cells). The transfected cells were seeded in glass-base dishes (35-mm in
840 diameter with a 12-mm diameter glass window, 0.15-mm-thick glass; Iwaki, Tokyo; 2×10^5
841 cells/dish) and cultured for 24-48 h before fluorescence microscopy observations. All
842 microscope observations were performed at 37°C by placing the entire microscope, except
843 for the far ends of the excitation arms and the detection arms, in a home-built microscope

844 environment chamber made with thermo- and electric-field-insulating plastic sheets and
845 equipped with four heating circulators (SKH0-112-OT, Kokensya, Tokyo, Japan). The Ham's
846 F12 medium used for microscope observations was free of sodium bicarbonate and phenol
847 red, and buffered with 2 mM N-[tris(hydroxymethyl)methyl]-2-aminoethanesulfonic acid (TES,
848 Sigma-Aldrich) at pH 7.4 (called Ham's F12 observation medium).
849

850 **Cell treatments with agonists and FAM-Xpep-TATs**

851 U-50488, DAMGO, and SNC-80 (Sigma-Aldrich), agonists for KOR, MOR and DOR,
852 respectively, were applied to the cells in the same way. The agonists were dissolved in DMSO
853 (2 mM), and then diluted with Hanks' balanced salt solution (HBSS, Nissui) buffered with 2
854 mM TES at pH 7.4 (T-HBSS), at a final concentration of 200 μM. The agonist solution (1 μl)
855 was added to the cells in 1 ml Ham's F12 observation medium (a final concentration of 200
856 nM) at 37°C.
857 For the cellular incorporation of FAM-Xpep-TATs (custom-synthesized by Cosmo-Bio),
858 the cells were first incubated with 150 μM pyrenebutyrate (Sigma-Aldrich) in T-HBSS at 37°C
859 for 5 min, and then 2 mM FAM-Xpep-TAT in T-HBSS was added at a final peptide
860 concentration of 20 μM. After an incubation at 37°C for 10 min, the cells were washed three
861 times with T-HBSS, and then fresh Ham's F12 observation medium was added to the cells.
862 The presence of FAM-Xpep-TAT in the cytoplasm was confirmed by the addition of the
863 membrane-impermeable quencher, trypan blue.[82]
864

865 **Fluorescence labeling of ORs**

866 The SNAPf-tagged wild-type and mutant ORs expressed in the PM (SNAPf tag located at the
867 extracellular N-terminus) were covalently conjugated by simultaneously incubating the cells
868 with two fluorescent SNAP ligands, SNAP-Surface 549 (New England Biolabs) and SNAP-
869 CF660R (Shinsei Kagaku), both at 300 nM, in the growth medium at 37°C in the CO_2
870 incubator for 30 min. The cells were washed three times with fresh medium (5-min
871 incubation each time), and then the Ham's F12 observation medium was added. The labeling
872 efficiency was determined by using the SNAPf-CD47-mGFP protein expressed in the PM. CD47
873 is a monomeric 5-pass transmembrane protein expressed in the PM.[83] We could not use ORs

874 for this purpose because they form transient dimers, and thus employed a monomeric CD47
875 (Supplementary Fig. 1c, d).
876 The labeling efficiency (the percentage of the SNAPf-tag protein labeled with the
877 fluorescent SNAP ligand) was determined in the following way. The percentage of fluorescent
878 mGFP spots of SNAPf-CD47-mGFP that was colocalized by the SNAP-dye spots were
879 measured as a function the concentration of the SNAP-dye-conjugated ligand in the medium,
880 after a 30 min incubation at 30°C. Note that not every mGFP molecule was fluorescent, but
881 since we examined whether the fluorescent mGFP molecule identified in the image was
882 colocalized by a SNAP-dye spot, the labeling efficiencies of the SNAPf-protein tag can be
883 evaluated without the influence of the fluorescence efficiency of mGFP. Then the efficiency at
884 each fluorescent ligand concentration was plotted against the dye concentration
885 (Supplementary Fig. 1e). We found that the plot could be fitted by a function of a single
886 exponential function plus a constant, providing the saturating labeling efficiency (constant)
887 and the characteristic labeling efficiency (exponential constant).
888 To obtain the labeling efficiency at a dye concentration of 300 nM for an incubation
889 period of 30 min, the conditions used throughout this study, the determined exponential
890 function was used for a concentration of 300 nM. The fluorescence labeling efficiencies under
891 our normal observation conditions were found to be 60% and 61% for SNAP-Surface 549 and
892 SNAP-CF660, respectively.
893
894 **Single fluorescent-molecule imaging**
895 Fluorescently labeled ORs expressed in the bottom PM (the PM facing the coverslip) at
896 fluorescent-spot number densities of 0.5 ± 0.25 spots/μm^2 for each color (SNAP-Surface 549
897 and SNAP-CF660R; total spot number densities of 1.0 ± 0.5 spots/μm^2; for conciseness, we
898 describe the number densities as ≈1 spot/μm^2 throughout this report) were observed at the
899 level of single molecules at 37°C, using a home-built objective lens-type TIRF microscope
900 constructed on an inverted microscope (Olympus IX-83), with a 100x, 1.49 numerical
901 aperture (NA) objective lens, optimized for the present research based on the instrument
902 used previously.[44, 84] ORs tagged with fluorescent probes were excited with TIR illumination
903 using the following power densities: SNAP-Surface 549 at 561 nm (Coherent OBIS 561-100

904 LS) at 0.35 μW/μm^2; and SNAP-CF660R at 642 nm (Omicron LuxXPlus 640-140) at 0.52
905 μW/μm^2. The dual-color images were separated by a dichroic mirror ZT405/488/561/640rpc-
906 UF3 (Chroma) and projected into two detection arms with band-pass filters of 572.5-647.5
907 nm (ET600/50m; Chroma) for the SNAP-Surface 549 dye and 662.5-737.5 nm (ET700/75m;
908 Chroma) for the SNAP-CF660R dye. In some experiments using mGFP-Xpeps and FAM-Xpep-
909 TATs, an additional detection arm equipped with a dichroic mirror ZT405/488/561/640rpc-
910 UF3 (Chroma) and a band-pass filter of 500.0-550.0 nm (ET525/50m; Chroma) was
911 employed. The fluorescence signal in each channel was first detected and amplified by a two-
912 stage microchannel-plate image intensifier (C9016-02MLP24; Hamamatsu Photonics), and the
913 intensified image was projected onto the scientific CMOS camera (C11440-22CU; Hamamatsu
914 Photonics), operated at 30 Hz, which was synchronized with the same intensifier-camera
915 set(s) placed on another detection arm. The image sequences in each channel were
916 superimposed after correction for spatial distortions, as described previously.[44] The positions
917 (x and y coordinates) of all of the observed single fluorescent-molecules were determined by
918 an in-house computer program, as described previously.[85]
919
920 **Evaluating colocalization durations**
921 The colocalization of two fluorescent molecules was defined as the event where two
922 fluorescent spots, representing these molecules, become localized within 200 nm of each
923 other, as described previously.[37, 44] Briefly, in single-color experiments using SNAP-Surface
924 549 (Supplementary Fig. 2), a spatial cross-correlation analysis was employed.[37] Using this
925 method, we found that when two fluorescent spots, each representing a single molecule of
926 SNAP-Surface 549, are located close together, the threshold distance for discriminating one
927 or two spots occurred at 200 nm in the present experimental set up. Using this definition,
928 colocalized trajectories were obtained and colocalization durations were estimated. In
929 simultaneous two-color single fluorescent-molecule tracking experiments, using the dye pairs
930 of SNAP-Surface 549 and SNAP-CF660R, the distance between the two molecules was directly
931 measured from the locations (x, y-positions) of each molecule (with different colors). Even
932 when examining pairs of different-colored molecules that are known to be truly associated,
933 the probability of scoring the two molecules as associated is limited by the localization

934 accuracies of each molecule and the accuracies of superimposing the two images. Based on
935 the method developed previously[44] and the accuracies determined here, we found that, for
936 truly associated molecules, the probability of scoring the two molecules as associated
937 increases to 99% when using the criterion that the molecules lie within 200 nm of each other.
938 Therefore, we used this criterion as the definition of colocalization in simultaneous two-color
939 single-molecule observations. This distance of 200 nm coincided with the definition of
940 colocalization in single-color experiments. Due to this coincidence, in the present research,
941 we defined the colocalization of two fluorescent molecules as the event where the two
942 fluorescent spots representing these molecules become localized within 200 nm from each
943 other.

944 Each time we found a green-magenta pair located within 200 nm (colocalization), we
945 measured the duration in which their distances remained within 200 nm (colocalized duration)
946 (for the results obtained by using two dye molecular species with different
947 excitation/emission wavelengths, we call them green and magenta probes/movies for
948 convenience in this report). After obtaining the colocalization durations for all of the
949 colocalization events, we generated a histogram (distribution) of colocalization durations. The
950 distribution of incidental colocalization durations was obtained by superimposing the magenta
951 image sequences with the 180-degree rotated (doubly flipped) green image sequences
952 (Supplementary Fig. 2d). For the precise analysis of these histograms, we first produced
953 cumulative histograms and fitted them with a single exponential function ($C_0 - C_1\exp[-t/\tau_1]$)
954 or the sum of two exponential functions ($C_0 - C_1\exp[-t/\tau_1] - C_2\exp[-t/\tau_2]$). The choice of the
955 number of exponentials (including the cases of the sum of three exponential functions) was
956 made based on Akaike's and Bayesian information criteria (they always agreed). Based on
957 these functions, the functions describing the original histograms were derived and overlaid on
958 the histograms.

959 First, we found that the distribution of incidental colocalization durations could be fitted
960 by a single exponential function, with a time constant representing the incidental
961 colocalization lifetime τ_{inci}. Second, the distribution of colocalization durations was obtained
962 for correctly superimposed magenta and green image sequences. This distribution could be
963 fitted by the sum of two exponential decay functions (τ_1 and τ_2; $\tau_1 < \tau_2$,). These results are

964 consistent with the theory developed here that predicts the distribution of colocalization
965 durations based on the diffusion equation (Supplementary Note 1). Since τ_1 was almost the
966 same as τ_{inci} (Fig. 1e), following the theory developed in Supplementary Note 1, τ_2 provided
967 the true homodimer lifetime (inverse of k_{off}; after correction for the trackable duration
968 lifetimes of the two fluorescent probes). The trackable duration lifetime is obtained from the
969 distribution of trajectory lengths, which would represent how long single molecules can be
970 continuously tracked under the influences of photobleaching and loss of signals due to
971 blinking and the entrance of the molecules into the PM areas located farther from the PM.
972 The distributions could be fitted as single exponential functions providing trackable duration
973 lifetimes (τ_{track}'s) of 16.3 ± 1.2 s (n = 500) for SNAP-Surface 549 and 7.8 ± 0.6 s (n = 400)
974 for SNAP-CF660R bound to SNAPf-MOR expressed in CHO-K1 cells observed at 30 Hz
975 (Supplementary Fig. 1f). The correction was made by using the equation:
976 $\tau(\text{corrected}) = [\tau(\text{observed})^{-1} - \tau_{track}(\text{dye 1})^{-1} - \tau_{track}(\text{dye 2})^{-1}]^{-1}$.
977
978 **Evaluating the colocalization index**
979 For the quantitative evaluation of the extent of colocalization (representing both the
980 frequency and lifetime of colocalization events) in simultaneous two-color single-molecule
981 imaging movies, we defined a parameter called the colocalization index. This analysis method
982 is essentially based on a pair cross-correlation analysis,[46] and the detailed method used in
983 this research is explained in Supplementary Fig. 2c-e and 3.
984
985 **Monte-Carlo simulations**
986 For the detailed method for Monte-Carlo simulations to examine the theory to obtain K_D from
987 the pair cross-correlation function (PCCF) (Supplementary Note 2), see the caption to
988 Supplementary Fig. 3.
989 The colocalization index depends on the number density of fluorescent spots in the PM.
990 In the present experimental observations, we selected the cells exhibiting fluorescent spot
991 number densities in the PM of 0.5 ± 0.25 spots/μm^2 for each color (SNAP-Surface 549 and
992 SNAP-CF660R; total spot number densities of 1.0 ± 0.5 spots/μm^2; for conciseness, we
993 describe the number densities as ≈1 spot/μm^2 throughout this report). These densities were

994 found to be reasonable by the Monte-Carlo simulation results, which indicated that, for the K_D
995 greater than 6.5 copies/μm^2, the colocalization index does not vary sharply in the number
996 density range of 0.5 - 1.5 spots/μm^2 (refer to Supplementary Fig. 3c). At the same time, we
997 developed the theory to evaluate the dimer-monomer dissociation equilibrium constant K_D
998 from the PCCF and the total number of spots in the image (refer to Supplementary Note 2).
999

1000 **Confocal imaging to study the effects of mGFP-Xpeps and FAM-Xpep-TATs on cells**
1001 **stably expressing ORs**

1002 CHO-K1 cells stably expressing ORs were transfected with mGFP-Xpeps. The cells were
1003 identified by the incubation with NucSpot Live 650 Nuclear Stain (Biotium), according to the
1004 protocol recommended by the manufacturer. After three washes with the complete medium,
1005 it was replaced with the Ham's F12 observation medium. The incorporation of the FAM-Xpep-
1006 TATs in the cells was performed as described in a previous subsection "Cell treatments with
1007 agonists and FAM-Xpep-TATs". Confocal fluorescence images were acquired on the same
1008 microscope station used for single-molecule imaging at 37°C, equipped with an Olympus
1009 SR10 spinning-disc confocal super-resolution unit (with a Plan-Apochromat 100x oil
1010 immersion objective; NA = 1.49).

1011 GFP and FAM were excited at 488 nm and detected through a 505-530 nm band pass
1012 filter. The NucSpot Live 650 was excited at 642 nm and detected through a 662.5-737.5 nm
1013 long pass filter. The concentrations of cytoplasmic mGFP-Xpep and FAM-Xpep-TAT were
1014 evaluated using calibration curves, obtained by observing the purified EGFP protein
1015 (BioVision) and FAM-Xpep-TATs dissolved in Ham's F12 observation medium at various
1016 concentrations, with a focus at 5 μm above the cover-glass surface (Supplementary Fig. 5b).
1017

1018 **Ca^{2+} mobilization assay**

1019 Since the OR expression level varies from cell to cell, the signaling process must be observed
1020 at the level of individual cells. The ORs are coupled to the inhibitory trimeric G protein Gi,
1021 which induces the decrease of the cytoplasmic cAMP concentration by inhibiting adenylyl
1022 cyclase. However, using the cells with low OR expression levels employed for single-molecule
1023 observations (≈1 fluorescent spot/μm^2), the decrease of the cytoplasmic cAMP levels in

1024 individual cells from those in non-stimulated state was impossibly difficult to measure.
1025 Meanwhile, the increase of the cytoplasmic Ca^{2+} concentrations by the PLCβ activated by the
1026 Gq signaling pathway could be measured in individual cells.[65, 66, 67] Therefore, in this assay,
1027 Gαq was modified so that OR could be coupled to Gαq. Namely, the C-terminal five amino-
1028 acid sequence of Gαq, ECGLY, was replaced with that of Gαi2, DCGLF (this chimeric protein is
1029 called Gqi5), because the Gα protein binds to the specific GPCR by way of its short C-terminal
1030 sequence.[86] Therefore, we generated the CHO-K1 cell line stably expressing Gqi5, had it
1031 express the OR, and then observed the cytoplasmic Ca^{2+} mobilization upon agonist addition,
1032 using the Ca^{2+}-sensitive dyes (Fig. 6c-f and Supplementary Fig. 1b). This method of using
1033 Gqi5 has been widely employed in the research of ORs[65] and other Gi-coupled GPCRs.[66]
1034 Briefly, CHO-K1 cells stably expressing Gqi5 were generated and transfected with the cDNAs
1035 encoding the wild-type and SNAPf-linked ORs. The Ca^{2+}-sensitive dyes Fluo-4 AM (Dojindo)
1036 and Rhod-3 AM (Thermo Fisher Scientific) were employed. Rhod-3 was used for the
1037 experiments with mGFP-Xpeps and FAM-Xpep-TATs, and Fluo-4 was used for the experiments
1038 that did not employ these homodimer-blocking reagents. These AM dyes were incorporated in
1039 the cell, according to the manufacturers' recommendations, using the following solutions: for
1040 Fluo-4, 4.6 μM Fluo-4 AM in T-HBSS containing 1.25 mM Probenecid (Dojindo) and 0.04 %
1041 (w/v) Pluronic F127 (Dojindo), and for Rhod-3, 10 μM Rhod-3 AM in T-HBSS containing 2.5
1042 mM Probenecid and 1× PowerLoad™ (Thermo Fisher Scientific). These loading solutions (2
1043 ml) were added to the cells and incubated in the dark at 37°C for 30 min, and then the cells
1044 were washed three times with T-HBSS.
1045 For the observations of the Ca^{2+} mobilization downstream of the SNAPf-tagged ORs, we
1046 selected cells expressing SNAPf-tagged ORs bound by SNAP-Surface 549 (or SNAP-CF660R
1047 for experiments using Rhod-3) at number densities of ≈1 fluorescent spot/μm^2 in the basal
1048 PM, using single-molecule detection (TIRF illumination) in the 561-nm channel (642-nm
1049 channel when we employed Rhod-3). These cells were then observed by epifluorescence
1050 illumination using the 488-nm channel to monitor the Fluo-4 signal (561-nm channel to
1051 observe the Rhod-3 signal and 488-nm channel for mGFP-Xpeps and FAM-Xpep-TATs).
1052 Agonist stimulation was performed by adding the DMSO solutions of agonists at a final
1053 concentration of 200 nM. To determine the saturation levels of the fluorescence signal

1054 intensity at higher concentrations of Ca^{2+}, 1 μM (final concentration) ionomycin (Wako) was
1055 added (which would increase the intracellular Ca^{2+} concentration to that outside the cells [1.3
1056 mM]). The Fluo-4 and Rhod-3 image sequences were analyzed using the ImageJ software.
1057 For the comparison of the functions of the SNAPf-ORs with those of the wild-type ORs,
1058 we hoped to compare the cells expressing the SNAPf-ORs at the levels of ≈1 spot/μm^2 in the
1059 basal PM with the cells expressing the wild-type ORs at levels comparable to or higher than
1060 those of SNAPf-ORs, because the cells expressing the wild-type ORs should serve as the
1061 positive controls. For this purpose, the expression levels of wild-type ORs were monitored by
1062 using cells transfected with the cDNA linking the wild-type OR sequence to the mCherry
1063 sequence via the self-cleavable 2A linker sequence (mCherry-2A-OR). This way, mCherry is
1064 released from the OR into the cytoplasm at the ER, and the wild-type OR is then transported
1065 to the PM. The expression of wild-type OR was detected by the presence of mCherry in the
1066 cytoplasm using the epi-illumination at 561 nm (sensitivities much lower than single-molecule
1067 imaging, showing the presence of rather high concentrations of mCherry). Therefore, the
1068 expression of the wild-type OR used in this study is considered higher than that of SNAPf-
1069 ORs.
1070

1071 **Software and statistical analysis**

1072 The microscope station that combined a single-molecule imaging system and a super-
1073 resolution confocal microscope was controlled by in-house LabVIEW2018-based software, and
1074 the single-molecule movie acquisitions were performed using the MCR software (Hamamatsu
1075 Photonics) for Windows. All statistical analyses for *in vitro* experiments were performed with
1076 Tukey's multiple comparison test except for the analysis of the colocalization lifetime data,
1077 which was performed with the Brunner-Munzel test, using OriginPro 2019b for Windows and
1078 RStudio 1.2.1335 for Windows. P values less than 0.05 were considered statistically
1079 significant. The confocal images were processed and analyzed using Image J for Windows.
1080 Curve fitting was performed by OriginPro 2019b for Windows. The simulation study was
1081 performed using the in-house software based on MATLAB 2019a for Windows.
1082

1083 **Data availability**

All data generated or analyzed for this study are available within the paper and its associated Supplementary Information. Any additional information required to reanalyze the data reported in this paper is available from the lead contact upon reasonable request. Superimpositions of image sequences obtained in two colors and tracking single-molecules for in-vitro observation data were performed using C++-based computer programs, produced in-house[87] and based on the well-established approaches. Further information regarding the experimental design may be found in the Nature Research Reporting Summary.

Code availability

Source codes for this have been integrated into a large, complex software package. While the software package cannot be extracted in a useful way, the entire software is available from the lead contact upon reasonable request, who will provide guidance on how to use it, as its manual and comments are written in Japanese.

Acknowledgements

We thank Profs. H. Takeshima of Kyoto University, R. Schülz of the University of Münich, R. Y. Tsien of the University of California San Diego, Simon J. Savis of the University of Oxford, Michiyuki Matsuda of Kyoto University, and M. Sokabe of Nagoya University, School of Medicine, for their kind gifts of cDNAs encoding rat KOR and DOR, that encoding rat MOR, that encoding mCherry, that encoding CD28, plasmids of pPBpuro and pCMV-mPBase, and the human T24 epithelial cell line, respectively. We also thank Ms. Irina Meshcheryakova for technical help in preparing the cDNAs. This work was supported in part by Japan Society for the Promotion of Science (JSPS) Grants-in-Aid for Scientific Research (Kiban A to A.K. [21H04772], Kiban S to A.K. [16H06386], Kiban B to T.K.F. [16H04775, 20H02585], Kiban C to R.S.K. [17K07333], Wakate B to R.S.K. [26870292], Wakate to T.A.T. [21K15058], and Challenging Exploratory Research to T.K.F. [18K19001] and A.K. [22K19334]), a Grant-in-Aid from the Ministry of Education, Culture, Sports, Science and Technology of Japan (MEXT) for Transformative Research Areas (A) to T.K.F. (21H05252), and a JST grant ACT-X to T.A.T. (JPMJAX211B). WPI-iCeMS of Kyoto University is supported by the World Premiere Research Center Initiative (WPI) of MEXT.

1114

1115 **Contributions**

1116 P.Z., R.S.K., and A.K. conceived and formulated the project. A.K., T.A.T., T.K.F., and P.Z.
1117 developed the simultaneous dual-color single-molecule tracking station. P.Z., T.A.T., R.S.K.,
1118 and A.K. designed biological experiments, and P.Z., with help from T.A.T., performed virtually
1119 all of the biological and microscopic experiments. T.K.F. developed and improved the in-house
1120 image analysis software. S.P. developed the theory for evaluating the k_{off} from the single-
1121 molecule experimental data (Note S1). K.M.H., T.A.T., and A.K. developed the colocalization
1122 index method, and T.A.T., Z.K., and A.K. developed the theory for linking the PCCF to the
1123 dimer dissociation equilibrium constant and performed Monte-Carlo simulations to prove the
1124 theory (Note S2). A.A. performed the OR sequence analysis to detect intrinsically disordered
1125 regions. A.K., P.Z., and T.A.T. wrote the manuscript, and all authors discussed the results and
1126 participated in the manuscript revisions.

1127

1128 **Competing interests**

1129 PZ and AK have a patent pending for Xpeps and Xpep-TATs. The remaining authors have no
1130 conflicts of interest to declare.

1131

References

1. Darcq, E., Kieffer, B.L. Opioid receptors: drivers to addiction? *Nat. Rev. Neurosci.* **19**, 499-514 (2018).

2. Valentino, R.J., Volkow N.D. Untangling the complexity of opioid receptor function. *Neuropsychopharmacology* **43**, 2514-2520 (2018).

3. Grimes, J., *et al.* Plasma membrane preassociation drives β-arrestin coupling to receptors and activation. *Cell* **186**, 2238-2255.e2220 (2023).

4. Schmid, C.L., *et al.* Bias factor and therapeutic window correlate to predict safer opioid analgesics. *Cell* **171**, 1165-1175.e1113 (2017).

5. Che, T., Roth, B.L. Molecular basis of opioid receptor signaling. *Cell* **186**, 5203-5219 (2023).

6. Hauser, A.S., Attwood, M.M., Rask-Andersen, M., Schiöth, H.B., Gloriam, D.E. Trends in GPCR drug discovery: new agents, targets and indications. *Nat. Rev. Drug Discov.* **16**, 829-842 (2017).

7. Spangler, S., Bruchas, M.R. Tuning biased GPCR signaling for physiological gain. *Cell* **171**, 989-991 (2017).

8. Bag, N., Wagenknecht-Wiesner, A., Lee, A., Shi, S.M., Holowka, D.A., Baird, B.A. Lipid-based and protein-based interactions synergize transmembrane signaling stimulated by antigen clustering of IgE receptors. *Proc. Natl. Acad. Sci. U.S.A.* **118**, e2026583118 (2021).

9. Cvejic, S., Devi, L.A. Dimerization of the delta opioid receptor: implication for a role in receptor internalization. *J. Biol. Chem.* **272**, 26959-26964 (1997).

10. He, L., Fong, J., von Zastrow, M., Whistler, J.L. Regulation of opioid receptor trafficking and morphine tolerance by receptor oligomerization. *Cell* **108**, 271-282 (2002).

11. Fujita, W., Gomes, I., Devi, L.A. Revolution in GPCR signalling: opioid receptor heteromers as novel therapeutic targets: IUPHAR review 10. *Br. J. Pharmacol.* **171**, 4155-4176 (2014).

12. Gomes, I., Gupta, A., Filipovska, J., Szeto, H.H., Pintar, J.E., Devi, L.A. A role for heterodimerization of μ and δ opiate receptors in enhancing morphine analgesia. *Proc. Natl. Acad. Sci. U.S.A.* **101**, 5135 (2004).

13. Jordan, B.A., Devi, L.A. G-protein-coupled receptor heterodimerization modulates receptor function. *Nature* **399**, 697-700 (1999).

14. Möller, J., *et al.* Single-molecule analysis reveals agonist-specific dimer formation of μ-opioid receptors. *Nat. Chem. Biol.* **16**, 946-954 (2020).

15. Ilien, B., *et al.* Pirenzepine promotes the dimerization of muscarinic M1 receptors through a three-step binding process. *J. Biol. Chem.* **284**, 19533-19543 (2009).

16. Liu, J., *et al.* Biased signaling due to oligomerization of the G protein-coupled platelet-activating factor receptor. *Nat. Commun.* **13**, 6365 (2022).

17. Gomes, I., *et al.* Identification of a μ-δ opioid receptor heteromer-biased agonist with antinociceptive activity. *Proc. Natl. Acad. Sci. U.S.A.* **110**, 12072 (2013).

18. Waldhoer, M., *et al.* A heterodimer-selective agonist shows in vivo relevance of G protein-coupled receptor dimers. *Proc. Natl. Acad. Sci. U.S.A.* **102**, 9050 (2005).

19. Kasai, R.S., Fujiwara, T.K., Kusumi, A. Metastable GPCR dimers trigger the basal signal by recruiting G-proteins. *bioRxiv*, 2020.2002.2010.929588 (2020).

20. He, S. Q., *et al.* Facilitation of μ-Opioid receptor activity by preventing δ-opioid receptor-mediated codegradation. *Neuron* **69**, 120-131 (2011).

21. Dijkman, P.M., *et al.* Dynamic tuneable G protein-coupled receptor monomer-dimer populations. *Nat. Commun.* **9**, 1710 (2018).

22. Ferré, S., Ciruela, F., Woods, A.S., Lluis, C., Franco, R. Functional relevance of neurotransmitter receptor heteromers in the central nervous system. *Trends Neurosci.* **30**, 440-446 (2007).

23. Fribourg, M., *et al.* Decoding the signaling of a GPCR heteromeric complex reveals a unifying mechanism of action of antipsychotic drugs. *Cell* **147**, 1011-1023 (2011).

24. George, S.R., O'Dowd, B.F., Lee, S.P. G-protein-coupled receptor oligomerization and its potential for drug discovery. *Nat. Rev. Drug Discov.* **1**, 808-820 (2002).

25. Navarro, G., *et al.* Evidence for functional pre-coupled complexes of receptor heteromers and adenylyl cyclase. *Nat. Commun.* **9**, 1242 (2018).

26. Meral, D., *et al.* Molecular details of dimerization kinetics reveal negligible populations of transient μ-opioid receptor homodimers at physiological concentrations. *Sci. Rep.* **8**, 7705 (2018).

27. George, S.R., *et al.* Oligomerization of mu- and delta-opioid receptors: generation of novel functional properties. *J. Biol. Chem.* **275**, 26128-26135 (2000).

1221 28. Wang, D., Sun, X., Bohn, L.M., Sadée, W. Opioid receptor homo- and heterodimerization
1222 in living cells by quantitative bioluminescence resonance energy transfer. *Mol. Pharmacol.*
1223 **67**, 2173-2184 (2005).
1224
1225 29. Asher, W.B., *et al.* Single-molecule FRET imaging of GPCR dimers in living cells. *Nat.*
1226 *Methods* **18**, 397-405 (2021).
1227
1228 30. Cechova, K., Lan, C., Macik, M., Barthes, N.P.F., Jung, M., Ulbrich, M.H. Kappa but not
1229 delta or mu opioid receptors form homodimers at low membrane densities. *Cell. Mol.*
1230 *Life Sci.* **78**, 7557-7568 (2021).
1231
1232 31. Drakopoulos, A., *et al.* Investigation of Investigation of inactive-state κ opioid receptor
1233 homodimerization via single-molecule microscopy using new antagonistic fluorescent
1234 probes. *J. Med. Chem.* **63**, 3596-3609 (2020).
1235
1236 32. Rogacki, M.K., *et al.* Dynamic lateral organization of opioid receptors (kappa, mu(wt)
1237 and mu(N40D)) in the plasma membrane at the nanoscale level. *Traffic.* **19**, 690-709
1238 (2018).
1239
1240 33. Gentzsch, C., *et al.* Selective and wash-resistant fluorescent dihydrocodeinone
1241 derivatives allow single-molecule imaging of μ-opioid receptor dimerization. *Angew.*
1242 *Chem. Int. Ed.* **59**, 5958-5964 (2020).
1243
1244 34. Calebiro, D., *et al.* Single-molecule analysis of fluorescently labeled G-protein–coupled
1245 receptors reveals complexes with distinct dynamics and organization. *Proc. Natl. Acad.*
1246 *Sci. U.S.A.* **110**, 743 (2013).
1247
1248 35. Hern, J.A., *et al.* Formation and dissociation of M1 muscarinic receptor dimers seen by
1249 total internal reflection fluorescence imaging of single molecules. *Proc. Natl. Acad. Sci.*
1250 *U.S.A.* **107**, 2693 (2010).
1251
1252 36. Kasai, R.S., Ito, S.V., Awane, R.M., Fujiwara, T.K., Kusumi, A. The Class-A GPCR dopamine
1253 D2 receptor forms transient dimers stabilized by agonists: detection by single-molecule
1254 tracking. *Cell. Biochem. Biophys.* **76**, 29-37 (2018).
1255
1256 37. Kasai, R.S., *et al.* Full characterization of GPCR monomer-dimer dynamic equilibrium by
1257 single molecule imaging. *J. Cell. Biol.* **192**, 463-480 (2011).
1258
1259 38. Zhou, P., *et al.* Single-molecule detection of transient dimerization of opioid receptors 2:
1260 Heterodimer blockage enhances morphine analgesia. *Companion paper* (2024).
1261
1262 39. Hernanz-Falcón, P., *et al.* Identification of amino acid residues crucial for chemokine
1263 receptor dimerization. *Nat. Immunol.* **5**, 216-223 (2004).
1264
1265 40. Jastrzebska, B., Chen, Y., Orban, T., Jin, H., Hofmann, L., Palczewski, K. Disruption of

1266 rhodopsin dimerization with synthetic peptides targeting an interaction interface. *J. Biol.*
1267 *Chem.* **290**, 25728-25744 (2015).
1268
1269 41. McMillin, S.M., Heusel, M., Liu, T., Costanzi, S., Wess, J. Structural basis of M3 muscarinic
1270 receptor dimer/oligomer formation. *J. Biol. Chem.* **286**, 28584-28598 (2011).
1271
1272 42. Petersen, J., *et al.* Agonist-induced dimer dissociation as a macromolecular step in G
1273 protein-coupled receptor signaling. *Nat. Commun.* **8**, 226 (2017).
1274
1275 43. Pan, Y. X. Expression of opioid receptors in mammalian cell lines. In: *opioid research:*
1276 *Methods and Protocols* (ed Pan ZZ). Humana Press (2003).
1277
1278 44. Koyama-Honda, I., *et al.* Fluorescence imaging for monitoring the colocalization of two
1279 single molecules in living cells. *Biophys. J.* **88**, 2126-2136 (2005).
1280
1281 45. Koyama-Honda, I., *et al.* High-speed single-molecule imaging reveals signal transduction
1282 by induced transbilayer raft phases. *J. Cell. Biol.* **219**, (2020).
1283
1284 46. Stone, M.B., Veatch, S.L. Steady-state cross-correlations for live two-colour super-
1285 resolution localization data sets. *Nat. Commun.* **6**, 7347 (2015).
1286
1287 47. Evans, E.J., *et al.* Crystal structure of a soluble CD28-Fab complex. *Nat. Immunol.* **6**,
1288 271-279 (2005).
1289
1290 48. Granier, S., *et al.* Structure of the δ-opioid receptor bound to naltrindole. *Nature* **485**,
1291 400-404 (2012).
1292
1293 49. Huang, W., *et al.* Structural insights into μ-opioid receptor activation. *Nature* **524**, 315-
1294 321 (2015).
1295
1296 50. Manglik, A., *et al.* Crystal structure of the μ-opioid receptor bound to a morphinan
1297 antagonist. *Nature* **485**, 321-326 (2012).
1298
1299 51. Wu, H., *et al.* Structure of the human κ-opioid receptor in complex with JDTic. *Nature*
1300 **485**, 327-332 (2012).
1301
1302 52. Ferré, S., *et al.* G protein–coupled receptor oligomerization revisited: functional and
1303 pharmacological perspectives. *Pharmacol. Rev.* **66**, 413 (2014).
1304
1305 53. Johnston, J.M., *et al.* Making structural sense of dimerization interfaces of delta opioid
1306 receptor homodimers. *Biochemistry* **50**, 1682-1690 (2011).
1307
1308 54. Mészáros, B., Erdős, G., Dosztányi, Z. IUPred2A: context-dependent prediction of protein
1309 disorder as a function of redox state and protein binding. *Nucleic Acids Res.* **46**, W329-
1310 W337 (2018).

55. Erdős, G., Dosztányi, Z. Analyzing protein disorder with IUPred2A. *Curr. Protoc. Bioinform.* **70**, e99 (2020).

56. Xhani, S., *et al.* Intrinsic disorder controls two functionally distinct dimers of the master transcription factor PU.1. *Sci. Adv.* **6**, eaay3178 (2020).

57. Kusumi, A., Tsunoyama, T.A., Suzuki, K.G.N, Fujiwara, T.K., Aladag, A. Transient, nano-scale, liquid-like molecular assemblies coming of age. *Curr. Opin. Cell Biol.* **89**, 102394 (2024).

58. Inomata, K., *et al.* High-resolution multi-dimensional NMR spectroscopy of proteins in human cells. *Nature* **458**, 106-109 (2009).

59. Grasberger, B., Minton, A.P., DeLisi, C., Metzger, H. Interaction between proteins localized in membranes. *Proc. Natl. Acad. Sci. U.S.A.* **83**, 6258-6262 (1986).

60. Keppler, A., Pick, H., Arrivoli, C., Vogel, H., Johnsson, K. Labeling of fusion proteins with synthetic fluorophores in live cells. *Proc. Natl. Acad. Sci. U.S.A.* **101**, 9955-9959 (2004).

61. Smith, J.S., *et al.* Noncanonical scaffolding of Gαi and β-arrestin by G protein–coupled receptors. *Science* **371**, eaay1833 (2021).

62. Wess, J., Oteng, A.B., Rivera-Gonzalez, O., Gurevich, E.V., Gurevich, V.V. β-arrestins: structure, function, physiology, and pharmacological perspectives. *Pharmacol. Rev.* **75**, 854-884 (2023).

63. Zhou, X.E., *et al.* Identification of phosphorylation codes for arrestin recruitment by G protein-coupled receptors. *Cell* **170**, 457-469.e413 (2017).

64. Ménard, L.*, et al.* Synergistic regulation of beta2-adrenergic receptor sequestration: intracellular complement of beta-adrenergic receptor kinase and beta-arrestin determine kinetics of internalization. *Mol. Pharmacol.* **51 5**, 800-808 (1997).

65. Camarda, V., Calo', G. Chimeric G proteins in fluorimetric calcium assays: experience with opioid receptors. In: *Calcium Signaling Protocols* (eds Lambert DG, Rainbow RD). Humana Press (2013).

66. Han, Y., Moreira, I.S., Urizar, E., Weinstein, H., Javitch, J.A. Allosteric communication between protomers of dopamine class A GPCR dimers modulates activation. *Nat. Chem. Biol.* **5**, 688-695 (2009).

67. Yokoyama, T., Kato, N., Yamada, N. Development of a high-throughput bioassay to screen melatonin receptor agonists using human melatonin receptor expressing CHO cells. *Neurosci. Lett.* **344**, 45-48 (2003).

68. Hauser, A.S., *et al.* GPCR activation mechanisms across classes and macro/microscales. *Nat. Struct. Mol. Biol.* **28**, 879-888 (2021).

69. Zhou, Q., *et al.* Common activation mechanism of class A GPCRs. *Elife* **8**, (2019).

70. Mafi, A., Kim, S.K., Goddard, W.A., 3rd. Mechanism of β-arrestin recruitment by the μ-opioid G protein-coupled receptor. *Proc. Natl. Acad. Sci. U.S.A.* **117**, 16346-16355 (2020).

71. Koehl, A., *et al.* Structure of the μ-opioid receptor–Gi protein complex. *Nature* **558**, 547-552 (2018).

72. Che, T., Dwivedi-Agnihotri, H., Shukla, A.K., Roth, B.L. Biased ligands at opioid receptors: current status and future directions. *Sci. Signal.* **14**, eaav0320 (2021).

73. Violin, J.D., Crombie, A,L,, Soergel. D,G,, Lark, M.W. Biased ligands at G-protein-coupled receptors: promise and progress. *Trends Pharmacol. Sci.* **35**, 308-316 (2014).

74. Manglik, A. Molecular basis of opioid action: from structures to new leads. *Biol. Psychiatry.* **87**, 6-14 (2020).

75. De Neve, J., Barlow, T.M.A., Tourwé, D., Bihel, F., Simonin, F., Ballet, S. Comprehensive overview of biased pharmacology at the opioid receptors: biased ligands and bias factors. *RSC Med.Chem.* **12**, 828-870 (2021).

76. Schulz, R., Wehmeyer, A., Schulz, K. Opioid receptor types selectively cointernalize with G protein-coupled receptor kinases 2 and 3. *J. Pharmacol. Exp. Ther.* **300**, 376 (2002).

77. Fukuda, K., Kato, S., Mori, K., Nishi, M., Takeshima, H. Primary structures and expression from cDNAs of rat opioid receptor δ-and μ-subtypes. *FEBS Lett.* **327**, 311-314 (1993).

78. Shaner, N.C., Campbell, R.E., Steinbach, P.A., Giepmans, B.N.G, Palmer, A.E., Tsien, R.Y. Improved monomeric red, orange and yellow fluorescent proteins derived from Discosoma sp. red fluorescent protein. *Nat. Biotechnol.* **22**, 1567-1572 (2004).

79. Lindberg, F.P., Gresham, H.D., Schwarz, E., Brown, E.J. Molecular cloning of integrin-associated protein: an immunoglobulin family member with multiple membrane-spanning domains implicated in alpha v beta 3-dependent ligand binding. *J. Cell. Biol.* **123**, 485-496 (1993).

80. James, J.R., Oliveira, M.I., Carmo, A.M., Iaboni, A., Davis, S.J. A rigorous experimental framework for detecting protein oligomerization using bioluminescence resonance energy transfer. *Nat. Methods* **3**, 1001-1006 (2006).

81. Naruse, K., Sai, X., Yokoyama, N., Sokabe, M. Uni-axial cyclic stretch induces c-src activation and translocation in human endothelial cells via SA channel activation. *FEBS Lett.* **441**, 111-115 (1998).

82. Cowen, T., Haven, A.J., Burnstock, G. Pontamine sky blue: a counterstain for background autofluorescence in fluorescence and immunofluorescence histochemistry. *Histochemistry* **82**, 205-208 (1985).

83. Tsunoyama, T.A., *et al.* Super-long single-molecule tracking reveals dynamic-anchorage-induced integrin function. *Nat. Chem. Biol.* **14**, 497-506 (2018).

84. Murakoshi, H., *et al.* Single-molecule imaging analysis of Ras activation in living cells. *Proc. Natl. Acad. Sci. U.S.A.* **101**, 7317 (2004).

85. Fujiwara, T.K., *et al.* Confined diffusion of transmembrane proteins and lipids induced by the same actin meshwork lining the plasma membrane. *Mol. Biol. Cell.* **27**, 1101-1119 (2016).

86. Conklin, B.R., Farfel, Z., Lustig, K.D., Julius, D., Bourne, H.R. Substitution of three amino acids switches receptor specificity of Gqα to that of Giα. *Nature* **363**, 274-276 (1993).

87. Fujiwara, T.K., *et al.* Development of ultrafast camera-based single fluorescent-molecule imaging for cell biology. *J. Cell. Biol.* **222**, (2023).